



UNIVERSIDADE DA BEIRA INTERIOR
Engenharia

Calibration and Data Processing of Fast-Response Virtual Three-Hole Probes

Tânia Sofia Cação Ferreira

Dissertação para obtenção do Grau de Mestre em
Engenharia Aeronáutica
(Ciclo de estudos integrado)

Orientador: Prof. Doutor Francisco Brójo
Co-orientador: Prof. Doutor Sergio Lavagnoli

Covilhã, outubro de 2015

Para Lourdes Almeida Cruz,

“Eu não sou nada.

Nunca serei nada.

Não posso querer ser nada.

À parte disso, tenho em mim todos os sonhos do mundo.”

Fernando Pessoa

Acknowledgements

These five months of internship were an amazing experience and I would like to thank everyone working in the institute.

First of all, I would like to thank Professor Francisco Brójo for agreeing in having me as his master thesis student working outside of our university, for his support during this period and for his promptness in every reply.

I am very grateful to Professor Tony Arts for accepting me as a master thesis student in his department.

My deepest gratitude goes to Professor Sergio Lavagnoli for his constant guidance, support and patience during my second internship under his supervision in what was a very busy time for him.

I am obliged to Cis de Maesschalk who trusted me with his data, providing me all the information I needed to be able to carry on my assignment and was available every time I had any doubt regarding it.

I would like to thank Pierre Londers for his cheerful help in the lab.

I had the pleasure of getting to know several other students that I want to thank their friendship and kindness and for making this period so enriching and fun.

A heartfelt appreciation goes to the friends I left in Covilhã in what would be our last semester together. Thank you for this wonderful and intense five years, for being part of my life and supporting me even when we are miles away apart.

Finally, I am very grateful to my beautiful family, for their kindness, generosity and specially, for their ability to end my occasionally unexpected homesickness.

Abstract

Fast response pressure probes are a robust measurement technique to characterize time-resolved unsteady flow in turbomachinery. An extensive data-processing is necessary to fabricate the appropriate and crucial calibration data for the intended flow quantities range.

Final aerodynamic calibration is available due to post processing of static and angular calibration data of nine fast response probes with two different transducer devices.

Finally, an uncertainty analysis of pressure and sensor angle errors as well as pitch angle effect is made recurring to pressure values from angular calibration data.

Keywords:

Pressure measurements, fast-response probes, virtual three-hole probe, calibration, data processing, unsteady flows,

Resumo

A caracterização contínua no tempo do escoamento transiente presente no interior de turbomáquinas pode ser realizado por sondas de resposta rápida. Estes instrumentos permitem a implementação de uma técnica de medição robusta da pressão total e estática em função do tempo, assim como da direção do escoamento, se um número suficiente de sensores for utilizado.

Para o efeito, é necessário um extenso processamento de dados para gerar informação de calibração apropriados e cruciais para o intervalo de alcance das propriedades do escoamento desejadas.

A calibração aerodinâmica final é obtida após o processamento da calibração estática e dinâmica de nove sondas de pressão de resposta rápida com dois tipos diferentes de sensores.

Por fim, uma análise de incertezas quanto a erros de pressão e de posicionamento angular do sensor da sonda assim como o efeito do ângulo de arfagem é realizada recorrendo a valores de pressão dos dados de calibração angular.

Palavras-chave:

Medições de pressão, sondas de resposta rápida, sonda virtual três-sensores, calibração, processamento de dados, escoamento transiente

List of Contents

1	Introduction	1
1.1.	Motivation.....	1
1.2.	Pressure Measurements in Turbines	2
1.3.	Research Objectives and Thesis Outline	4
2	Generalities in Pressure Measurements	7
2.1.	Historical Note	7
2.2.	Types of Pressure Measurements	10
2.3.	Requirements of Pressure Probes	12
2.4.	Pressure Transducers.....	12
2.4.1.	Temperature Compensation.....	14
2.5.	Fast-Response Pressure Probes.....	16
3	FRAP Static and Angular Calibration Data Post-Processing	19
3.1.	Static Calibration	19
3.1.1.	Static Pressure Indicator Calibration	19
3.1.2.	In-situ Calibration	20
	CT-3 Facility and Test Conditions	20
	Run-Up/Run-Down.....	22
	Static Calibration of Transducers for Reference Five-Hole Pneumatic Pressure Probe ..	23
3.2.	Angular Calibration	25
3.2.1.	C-4 Facility and Experimental Set Up	25
3.2.2.	Yaw and Pitch Angle Measurement Sequences.....	26
3.2.3.	Flow Calibration Range.....	26
3.2.4.	Calibration Data Post-Processing	30
	Signal Acquisition.....	30
	Static Calibration Coefficients with Null Angle Total Recovery Assumption	32
	Shift Angle Correction	33
	Analysis of Pitch Fine Sequence	35
	Analysis of Yaw Angle Sequences	36
	General Flow Quantities.....	39
	Frequency Analysis	39
4	FRAP Aerodynamic Calibration.....	43
4.1.	Aerodynamic Calibration Script Description	43
	Flow Quantities Reconstruction.....	45
4.1.1.	Modifications to Aerodynamic Calibration Script	48
4.2.	Configuration Evaluation	50
4.2.1.	Angle Between Sensors.....	52
4.2.2.	Central Amplification Coefficient K_z	52

4.3.	Uncertainty Analysis.....	54
4.3.1.	Pressure Readings Error	55
4.3.2.	Sensor Angle Position Error	55
4.3.3.	Pitch Angle Error	56
4.3.4.	Combination of Possible Errors	57
5	Conclusions	59
6	Recommendations for Future Work	61
7	List of References	63

List of Figures

Figure 1.1: First patented turbojet engine (left) and a relatively recent turbofan engine (right)	1
Figure 1.2: Brayton cycle: (left) pV diagram, (right) Ts diagram	2
Figure 1.3: (left) Three-dimensional flow feature in an axial turbine rotor passage and (right) stator wake development in a downstream rotor passage	3
Figure 2.1: Pitot pressure tube illustration	7
Figure 2.2: Tip of one-sensor Pitot probe of 0.84 mm diameter	8
Figure 2.3: Virtual four sensor probe.....	9
Figure 2.4: Wedge fast-response pressure probe.....	9
Figure 2.5: High temperature fast-response pressure probe with a 2.5 mm diameter.....	10
Figure 2.6: Typical piezo-resistive transducer.....	13
Figure 2.7: Passive temperature compensation: (left) stainless cylinder module (right) internal circuitry	14
Figure 2.8: Step and stability test for a passive temperature compensated FRAP for flow at temperature of: 297 K (left) and 313K (right)	15
Figure 2.9: Step and stability test for a FRAP: without any temperature compensation (left) and with a passive compensation (right)	15
Figure 2.10: (a) bare piezo-resistive gauge picture, (b) implementation of a Kulite® gauge in a Pitot probe with a protective silicon layer and (c) active temperature compensation circuitry.....	16
Figure 2.11: Transducers drawings: Kulite® XCQ-062 (left) and Measurement Specialties™ EPIH-11 (right).....	17
Figure 2.12: Kulite sensor FRAP: illustration and photograph (left) and comparison of change of lift and dynamic errors for different geometries (right)	17
Figure 3.1: Lateral view of CT3	21
Figure 3.2: Typical test conditions in the CT-3.....	21
Figure 3.3: Pressure and rotational speed (left) and temperature (right) during in-situ calibration.....	22
Figure 3.4: In-situ calibration of FRAP voltage signals with reference pneumatic pressure probe	23
Figure 3.5: Measurement chain of reference pressure transducers.....	24
Figure 3.6: C-4 facility: photograph (left) and lateral view drawing (right)	25
Figure 3.7: Angular calibration reference yaw and pitch angle	26
Figure 3.8: FRAP voltage signals, temperature and pressure during yaw angle calibration ...	31
Figure 3.9: Pressure and temperature sensitivity voltage signals.....	32
Figure 3.10: New FRAP's static calibration coefficients.....	33
Figure 3.11: FRAP measured pressure for yaw angle	34

Figure 3.12: Pitch angle influence in flow recovery	35
Figure 3.13: Pressure measurements at different Mach numbers	37
Figure 3.14: Ratio of root-mean-square and mean pressure	37
Figure 3.15: FRAP recovery factor of calibration flow	38
Figure 3.16: Calibration flow pressure, temperature and Reynolds number range	39
Figure 3.17: Frequency analysis of FRAP's pressure signal	40
Figure 3.18: Strouhal number for FRAP's Reynolds number operating range	41
Figure 4.1: 3D maps of aerodynamic calibration coefficients	45
Figure 4.2: Virtual three sensor probe pressure measurements	46
Figure 4.3: Zonal calibration map	47
Figure 4.4: Flow quantities reconstruction with aerodynamic calibration script	48
Figure 4.5: Three FRAP's imposed and retrieved flow quantities	49
Figure 4.6: Three FRAP's error in flow quantities reconstruction	50
Figure 4.7: Zonal calibration map for different angles between sensors	52
Figure 4.8: Zonal calibration map for different central amplification coefficients.....	53
Figure 4.9: Flow quantities error for different central amplification coefficients.....	54
Figure 4.10: Flow quantities error for pressure readings error of ± 5 mbar	55
Figure 4.11: Flow quantities error for sensor position error of $\pm 5^\circ$	56
Figure 4.12: Flow quantities error for pitch angle variation of $\pm 30^\circ$	57
Figure 4.13: Flow quantities error for combined known sources of errors	58

List of Tables

Table 2.1: List of pressure probes and dimensions.....	18
Table 3.1: FRAP's initial static calibration coefficients	20
Table 3.2: Static calibration coefficients of reference transducers.....	24
Table 3.3: Flow calibration range.....	28
Table 3.4: List of angular calibration tests.....	30
Table 3.5: New static calibration coefficients	33
Table 3.6: Shift and separation averaged angles	34
Table 3.7: Flow characteristics.....	39
Table 4.1: Angular calibration list by Mach number and measuring sequence	51
Table 4.2: Average and maximum flow quantities error for inserted pressure, sensor and pitch angle variation	58

Nomenclature

Roman symbols

C	Sutherland temperature constant [120 K]
D	probe diameter [m]
f	frequency [Hz]
f _s	sampling frequency [Hz]
F _D	drag force [N]
K _{Mach}	Mach number calibration coefficient [-]
K _{yaw}	yaw angle calibration coefficient [-]
K _{tot}	total pressure calibration coefficient [-]
K _{dyn}	dynamic pressure calibration coefficient [-]
k _z	central sensor amplification coefficient [-]
L	probe length [m]
M	Mach number [-]
p	pressure [Pa]
q	dynamic pressure [Pa]
R	specific gas constant [287.05307 m ² /s ² K]
R ²	coefficient of determination [-]
Re	Reynolds number [-]
St	Strouhal number [0.21]
T	temperature of the flow [K]
T _{ref}	Sutherland reference temperature [291.15 K]
U	gas velocity at the nozzle [m/s]

Greek symbols

γ	air specific heats ratio [1.4]
μ	dynamic viscosity [kg/m/s]
μ _{ref}	Sutherland reference dynamic viscosity [1.827·10 ⁻⁵ Ns/m ²]
θ	pitch angle [°]
ρ	volumetric mass density of the flow [kg/m ³]
ψ	yaw angle [°]

Subscripts

acq	acquired
-----	----------

atm	atmospheric
C	pressure probe central sensor
L	pressure probe left sensor
nozzle	nozzle outlet flow
o	total/stagnation
R	pressure probe right sensor
s	static
targ	target

Acronyms

C-4	Calibration facility
CT-3	Isentropic compression tube annular cascade facility
FRAP	Fast response aerodynamic probe
PSD	Power Spectral Density
RMS	Root Mean Square
RPM	Revolutions per Minute
VKI	The von Kármán Institute for Fluid Dynamics

1 Introduction

1.1. Motivation

Over relatively recent years, experimental and numerical research on turbomachinery performance has provided important information to significantly improve engine's reliability and efficiency, Figure 1.1.

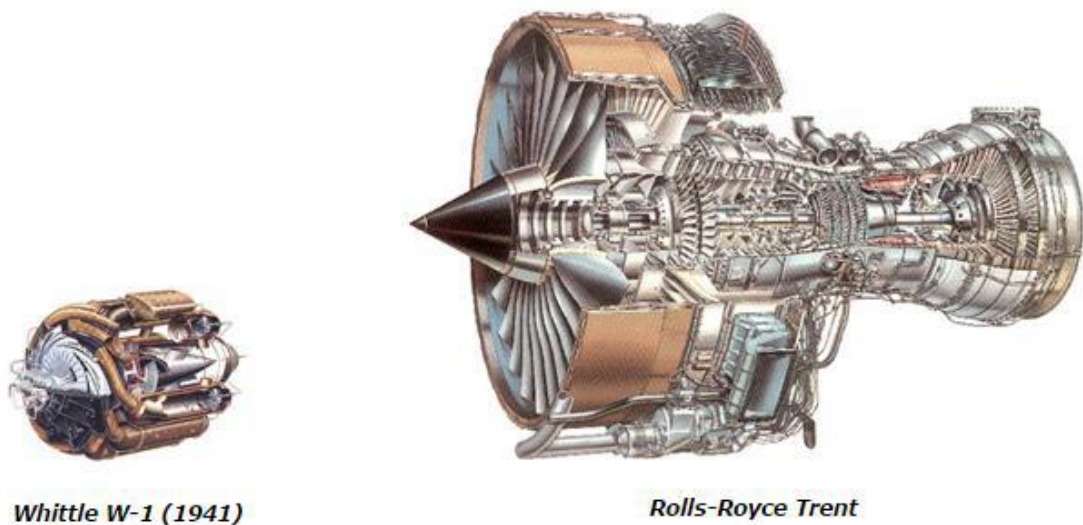


Figure 1.1: First patented turbojet engine (left) and a relatively recent turbofan engine (right) [picture from MIT Gas Turbine Laboratory website]

As described in (Kupferschmied, et al. 2000) turbomachinery flows are highly unsteady due to the relative motion of rotating and fixed blade rows and periodic fluctuations arise from the regular passing of wakes and other non-uniformities, such as secondary and leakage flow patterns or shocks over the blades.

Stochastic fluctuations can be also due to turbulence, to unsteady transition and separation of boundary layers or to intermittent blade flutter. All these unsteady effects have to be detected by measurement systems in order to understand the loss mechanisms and unsteady running conditions.

Characterization of the flow inside the turbine with knowledge of pressure and temperature distribution can also determine the thermodynamic limits of its design. Such helps prevent damages and achieve a longer lifetime of the turbine's components and the turbine as a whole.

Optimization of this component is therefore a major factor on extending the engine's durability.

Moreover, bearing in mind the existing environmental issues and ongoing growth of aviation industry and transportation volume, it becomes of the utmost importance to reduce fuel consumption and global emissions.

1.2. Pressure Measurements in Turbines

A gas turbine is a rotary engine that extracts energy from a flow of combustion gas. Energy is extracted in the form of shaft power, compressed air and thrust, in any combination, and is used to power the vehicle or power-plant.

The basic components of a gas are an upstream compressor coupled to a downstream turbine and a combustion chamber in between.

Energy is released when air is mixed with fuel and ignited in the combustor. The resulting gases are directed over the turbine's blades, spinning the turbine, and, cyclically, powering the compressor.

Finally, the gases are passed through a nozzle, generating additional thrust by accelerating the hot exhaust gases through an expansion back to atmospheric pressure. This cycle of continuous combustion is known as the Brayton cycle, Figure 1.2.

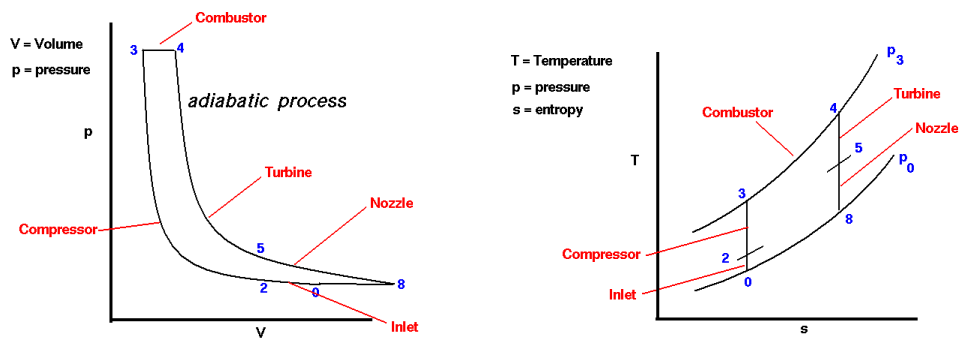


Figure 1.2: Brayton cycle: (left) pV diagram, (right) Ts diagram [pictures from NASA website]

It defines a varying volume sequence with four distinct stages: compression combustion, expansion and exhaust. The working gas is compressed and burned and work is produced by the expansion of the hot gas (Lenherr 2010).

The amount of generated work can provide an idea of the turbine's overall efficiency, which can also be determined through the evaluation of losses associated with unsteady flow field phenomena in turbomachines. On (Denton 1993) an extensive review of the loss generating mechanisms in turbomachinery is presented. Three main sources of loss in turbomachines

were identified: viscous effects in boundary layers and in mixing process, shock waves and heat transfer across temperature difference.

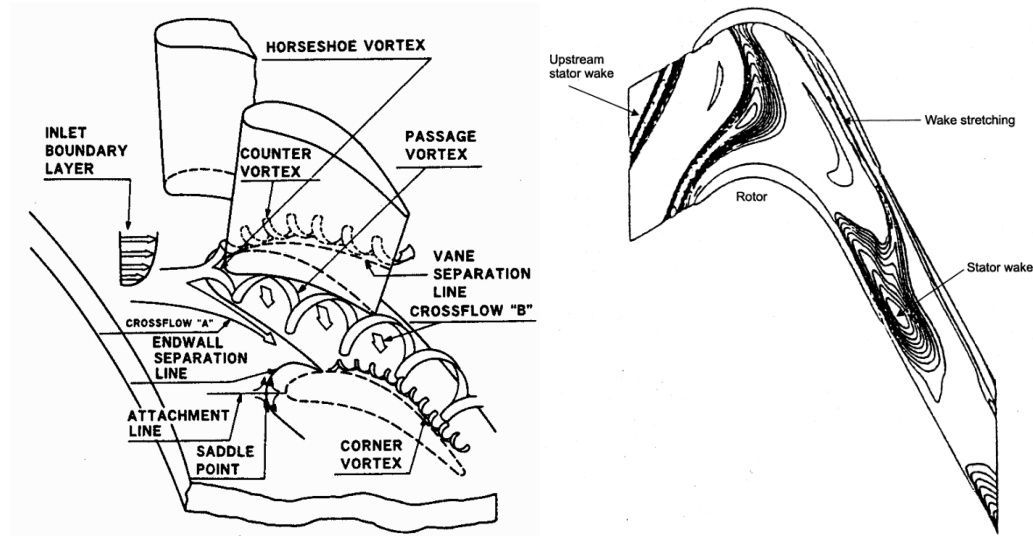


Figure 1.3: (left) Three-dimensional flow feature in an axial turbine rotor passage (Lenherr 2010) and (right) stator wake development in a downstream rotor passage (Pfau 2003)

Stagnation pressure loss coefficient is still very commonly used in the literature for evaluating the loss generation, in particular for compressor and turbine cascade experiments. This quantity depends on the frame of reference and is therefore not suitable in machines where the relative stagnation pressure and stagnation temperature can change. The reason that the stagnation pressure loss coefficient is still so commonly used is that it can be directly measured with aerodynamic probes, whereas the entropy is derived from pressure and temperature measurements and therefore much more complicated to derive (Mansour 2009).

Flows in turbomachinery require very specialized instrumentation due to its highly unsteady nature with large velocities and significant fluctuations and, also worth mentioning, difficult accessibility inside the turbomachine.

On (Lenherr 2010) an overview of measurement techniques available in turbomachines is presented, separating those that are invasive, i.e. where the device is inserted in the flow inducing disturbances in it, from non-invasive methods. For pressure measurements, available techniques are listed below:

Hot wire anemometry: this probe contains a resistance heated by an electronic circuit and if kept constant, through an indirect relationship to temperature, this intrusive method measures time-resolved flow velocity, which cools down the wire.

Laser Doppler anemometry: it is a non-intrusive technique and gives information about flow velocity. It is mostly used on applications with reversing flow, chemically

reacting or high-temperature media and rotating machinery, where physical sensors are difficult or impossible to use.

Pneumatic probes: are only able to measure time-averaged pressure due to pneumatic damping between the pressure taps and the pressure transducers (Mansour 2009). Considering flow in turbomachines is mainly unsteady, the need for a time-resolved flow characterization was answered with the development of fast response pressures probes which don't require a pneumatic line.

Fast response aerodynamic probes: a small and robust probe is inserted in the flow field, thus it is classified as an intrusive device. The flow around the probe head generates a pressure field on the probe surface. This pressure depends on the head geometry and size as well as on the velocity and direction of the flow. At selected positions on the probe head, measurement holes are inserted to measure the corresponding pressures. This method needs at least one hole per flow quantity to be measured. Moreover, fast response aerodynamic probes satisfy all the turbomachinery requirements and, contrarily to the other measurement techniques, are able to provide time-resolved total and static pressure. This technique is the object of study for the present thesis and additional information is provided on section 1.1.

Progress in material science and improvement of cooling techniques as well as in computational tools and measurement techniques have led to the analysis and design of more powerful and efficient turbines (Lenherr 2010).

1.3. Research Objectives and Thesis Outline

The main focus of the present thesis is data processing of calibrations of fast response pressure probes for compressible unsteady flow in high pressure turbines for testing a transonic fully annular cascade wind tunnel.

The present thesis is organized in six chapters which describe the development, results and conclusions of the research work.

Chapter 1 delineates the motivation and main objectives of this work.

Chapter 2 offers the theoretical knowledge required for the full comprehension of pressure measurements.

Chapter 3 describes the data post-processing of static and angular calibration of fast-response pressure probes.

Chapter 4 reports on the numerical processing of the previous chapter results for the aerodynamic calibration of these measurement devices. Calibration maps are produced for

further evaluation and reconstruction of unknown flow from pressure measurements. An uncertainty analysis of present effects in flow quantities retrieval is also depicted.

At last, chapter 5 summarizes the main conclusions and chapter 6 contains some future work suggestions.

2 Generalities in Pressure Measurements

2.1. Historical Note

Anderson depicts in his book (Anderson Jr. 1997) that experimental aerodynamics had their real start in the late seventeenth century, mainly due to Henry Pitot's invention, still praising some prior small contributions of da Vinci and Mariotte. This honour is attributed for his hollow bent tube able to measure locally the stagnation pressure while facing the flow perpendicularly, which was later on validated also for flow velocity calculation by Bernoulli's equation, Figure 2.1.

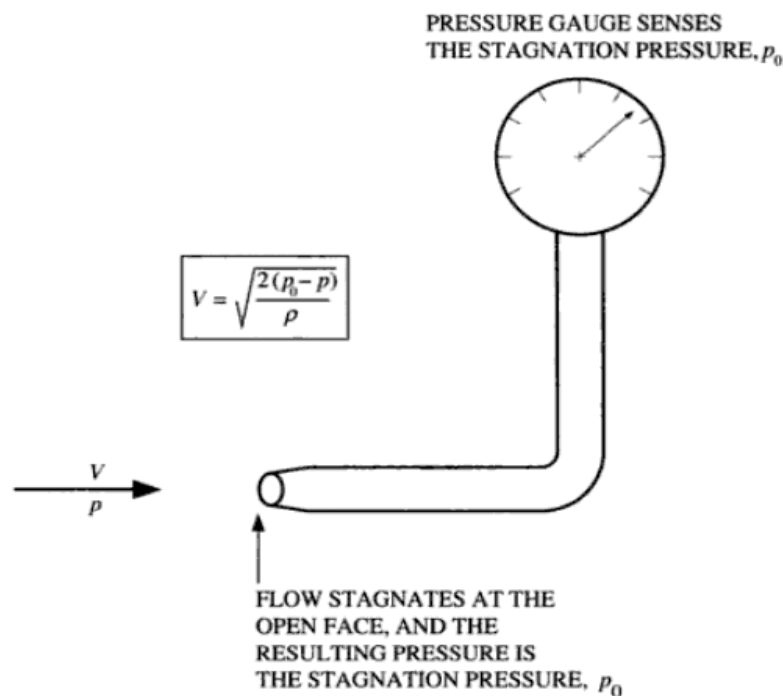


Figure 2.1: Pitot pressure tube illustration (Anderson Jr. 1997)

This marked a starting point from which pressure probes have been developed over the years. Pneumatic pressure probes allowed the determination of flow quantities such as total pressure, static pressure, Mach number and flow angles if a sufficient number of taps was used. Characterization of 2D and 3D flow is possible nowadays, provided that a minimum of three or four/five sensor pressure measurements, respectively, are combined together. However, due to signal damping resulting from the pneumatic lines between the tip bores and the pressure transducers confined this technique to time averaged flow information only. Of course, this is a severe limitation regarding the unsteady and complex nature of turbomachinery flows, which rather demands a continuous measurement at several points in

space with a bandwidth sufficient to determine the physical flow quantities of interest (Kupferschmied, et al. 2000).

Fortunately, the miniaturization of pressure transducers allowed a higher proximity of these devices to the probe taps, significantly improving their dynamic characteristics. Further research and technological advances led to development of fast response pressure probes, able to provide time-resolved flow measurements.

A good example of the success of sensors' miniaturization is the development of a 0.84 mm diameter one sensor pitot probe, displayed on Figure 2.2, however, it is unsuitable in inter-stage turbomachines measurements due to lack of space.



Figure 2.2: Tip of one-sensor Pitot probe of 0.84 mm diameter (Kupferschmied, Gossweiler and Gyarmathy 1994)

A virtual four sensor fast response aerodynamic probe is developed at the ETH Zurich. More explicitly, this concept combines pressure measurements from two single sensor probes to reconstruct time-resolved three-dimensional flow. One probe makes three acquisitions at different yaw angles, similar to a common virtual three sensor probe. The novelty is the use of a second probe with a 45° pitch angle sensor to characterize the flow in both directions (Pfau, et al. 2002).

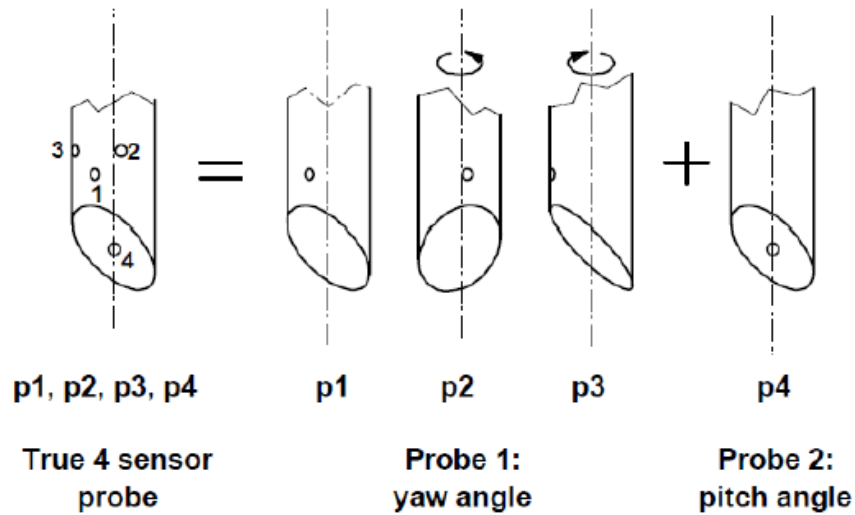


Figure 2.3: Virtual four sensor probe (Pfau, et al. 2002)

A three sensor wedge probe was developed at the VKI to measure unsteady flow in a transonic turbine. Advantages of this configuration are high angular sensitivity offered by a 60° angle between sensors and a good dynamic response due to the absence of line cavity, however it faces circulation induced lift and dynamic stall. Detailed information on this technique can be found in (Delhay, et al. 2010).

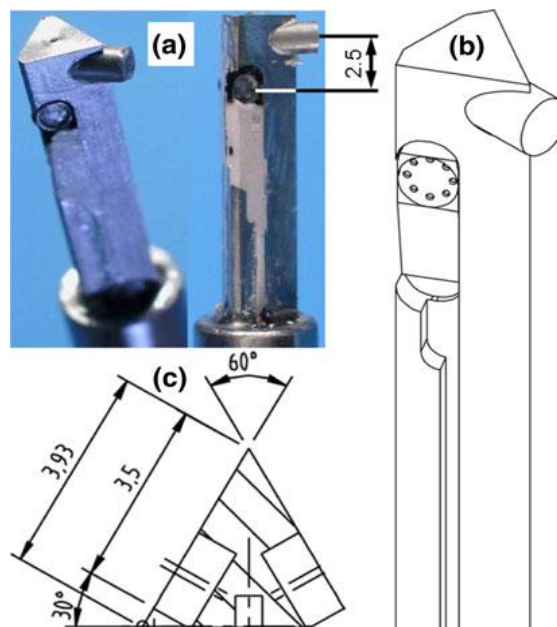


Figure 2.4: Wedge fast-response pressure probe (Delhay, et al. 2010)

A high temperature fast-response probe is developed, built and tested in (Lenherr 2010) and it is able to withstand flows with temperatures up to 533K, Figure 2.5. Although it has a considerable diameter of 2.5 mm, it is nonetheless an important contribution for

turbomachinery applications considering their high temperature flows and also that this instrumentation technology was limited to flow temperatures of 393K.



Figure 2.5: High temperature fast-response pressure probe with a 2.5 mm diameter (Lenherr 2010)

In sum, space shortage within a turbomachine stator-rotor interval demand a continuing miniaturization of this measurement technique in order to fully characterize its highly unsteady three-dimensional flows.

2.2. Types of Pressure Measurements

In order to properly design a turbomachine and/or optimize its components, it is helpful to attain an accurate knowledge of the flow field to which it will be subjected, to determine velocity fields and evaluate losses and performances of work absorbing or producing machinery.

In sum, a pressure measurement campaign should be chosen accordingly to the target turbomachine component and to the intended flow quantities one wants to characterize.

There are different types of pressure measurements depending on the measurement task and they can be made individually or combined in the same probe.

For instance, static pressure is the pressure exerted by a fluid that is independent of its velocity. It is equal in all the directions and it is measured perpendicularly to the flow.

Total pressure is obtained by isentropically decelerating the flow to rest, thus being also named stagnation pressure. Pitot probes are used to measure this pressure, which corresponds to the sum of static and dynamic pressure:

$$p_o = p_s + \frac{1}{2}\rho U^2 \quad (2.1)$$

The accuracy of total pressure measurements depends on several effects, some of which are outlined in (Anthoine, et al. 2009) such as incidence, Reynolds and Mach number, velocity gradients, wall proximity, flow unsteadiness and probe geometry.

Additionally, it is possible to measure dynamic pressure directly by adding static ports to a pitot probe, named hereafter a pitot-static probe. This characterization of flow velocity is made through the placement of a transducer between total and static pressure channels and its differential response will provide the dynamic pressure.

Finally, flow direction measurements give a more complete knowledge of the flow field providing also the yaw angle and/or pitch angle, depending on the sensors' number and placement.

Flow direction measurements oblige the use of more than one pressure acquisition and can be achieved by choosing the more appropriate of two different methods explained in (Bryer and Pankhurst 1971).

On rotating a multi-hole probe until almost the same pressure is acquired at each lateral hole, equilibrium is achieved, thus naming this method *equi-balanced*. According to the probe's geometry, the flow direction can be described through its aligned angular position. In spite of its easier application and non-requiring calibration, this method cannot be implemented in turbomachinery measurements due to the short available space and constant change in flow direction.

Lastly, in the second method the probe is held stationary and it records the unknown flow pressure fluctuations, hence previous calibration is indispensable to link these pressure measurements to the target flow quantities. For the present work this is the method used for flow direction and Mach number characterization inside the turbine test rig.

2.3. Requirements of Pressure Probes

In (Gossweiler 1996) a thorough research of requirements and limitations of fast response probes in turbomachinery is presented. Even considering the differences in flow conditions from one turbomachine to another, the following parameters should be fully optimized due to the general unsteadiness of the flow:

Frequency response: limits the characterization of flow fluctuating phenomena. Considering the periodic flow fluctuating nature and blade passing frequency, it should be at least above 10 kHz.

Spacial resolution: in order to resolve details in flows the probes must be significantly smaller than the flow structure under study. Hence, miniaturization of pressure probes is of the utmost importance. Moreover, dynamic aerodynamic errors and flow disturbances are also significantly reduced.

Accuracy: this factor will determine the degree of reliability on the pressure measurements and keep systematic errors to a minimum.

Resolution and signal-to-noise ratio: both these parameters limit the smallest change that can be detected, a necessity for a more detailed reconstruction of flow direction and velocity variations during an engine operation.

Pressure and temperature level: in turbine testing, pressures range from vacuum to several bar and this can be detected by existing probes. However, the problem lies on their relatively low temperature operation, compared with the one present in flows in turbomachines.

Optimizing spacial resolution will help reduce probe blockage effect, which is defined as the ratio of the probe stem frontal area to the *channel* area. Such effect is a function of Mach number, probe stem thickness, distance to upstream blade row, probe immersion depth and wall proximity.

Blockage effects will result in an increase of Mach number and a decrease of static pressure in closed-wall wind tunnels. For continuity reasons the presence of the probe will create an overspeed in its close vicinity inducing measurement errors (Brouckaert 2014).

Once again, the further miniaturization of this method is underlined.

2.4. Pressure Transducers

The design of a pressure probe has to take into account the dimensions of the location where it will be used, the required response frequency and sensitivity, and its external dimensions, amongst others. The majority of these factors are constrained by the probe's transducer, which must be chosen accordingly.

In terms of working principle, pressure transducers can be piezo-electric, piezo-resistive, capacitance or optical fiber sensors, amongst others.

Fast-response pressure probes of the present assignment employ piezo-resistive sensors which have lighter weight, smaller size, higher output and higher frequency of response compared to the other types of transducers (Brouckaert 2014).

Piezo-resistive transducers employ a silicon strain gauge sensor to produce an electrical output that is proportional to the pressure on its sensing surface.

Electrical pressure transducers can be divided in two types: active or passive devices. Transducers used in the present assignment work under Wheatstone bridges principles falling into the passive device category. It generates an output voltage signal accordingly with the change of physical input sensed by the bridge. These types of transducers that detect small resistance changes in the bridge circuits are strain gage transducers, they transform a deformation (or a micro-displacement) into a resistance variation.

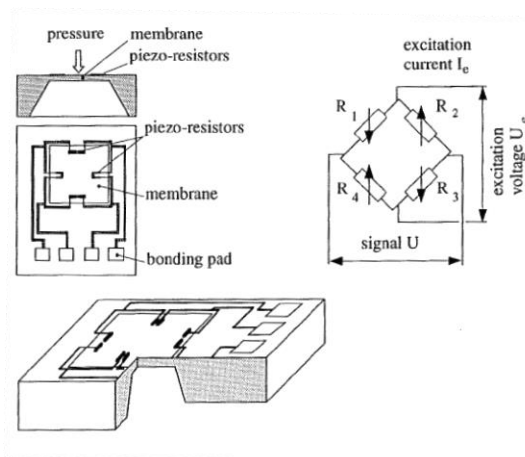


Figure 2.6: Typical piezo-resistive transducer (Gossweiler 1996)

Its downside is the high sensitivity to temperature changes that not only affects the resistivity of each gauge and thereby the transducer zero pressure output but also the bridge gauge factor (Brouckaert 2014), respectively it affects both the device's offset and gain. This sensitivity of the sensor to temperature changes can be approached either by a passive or by an active compensation both described in the following section 2.4.1.

As for the transducer insertion in the fast-response pressure probe, it can be subsurface mounted, protecting it from aggressive flow conditions, or it can be flush mounted, maintaining the frequency response. The latter is the configuration present in the current assignment pressure probes, more adequate for measuring rapidly varying pressure. In this arrangement the sensing membrane of the transducer is located directly on the surface where the pressure has to be measured, thus eliminating the need for a pressure tap and for

a plastic or metal tube connecting the tap to the inner cavity of the transducer. This exclusion of these elements significantly increases the response time of the pressure measuring system (Anthoine, et al. 2009).

2.4.1. Temperature Compensation

Due to resistivity variations and differential expansion as a consequence of Joule heating and ambient fluctuations, temperature variations highly affect the voltage output accordance with previous calibrations of transducers in pressure measurements.

Moreover, considering the large temperature transients probes of this present work will be subjected to, a compensation of this influence becomes mandatory.

Fortunately, at least two methods can be used to compensate for this temperature dependency: passive and active compensation.

In passive compensation, the typical approach is to add external resistors to the bridge, commercially provided by the manufacturer, and reduce the sensitivity of the bridge output to thermal influence, at the expense of an overall lower sensor output.

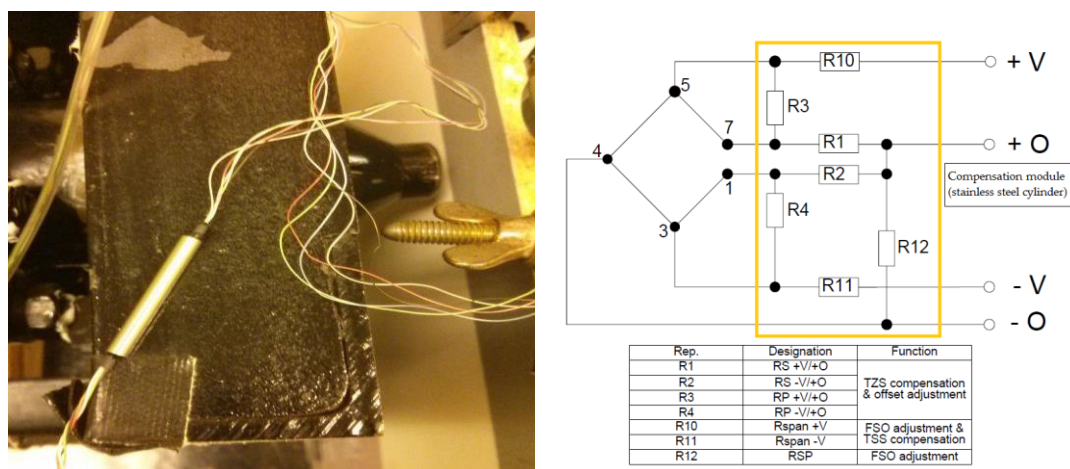


Figure 2.7: Passive temperature compensation: (left) stainless cylinder module (right) internal circuitry (García 2014)

Configuration displayed on Figure 2.7 is tested and compared with a non-compensated one on (García 2014) in a step and stability test used to evaluate temperature effects when subjected to steady flows at different temperatures.

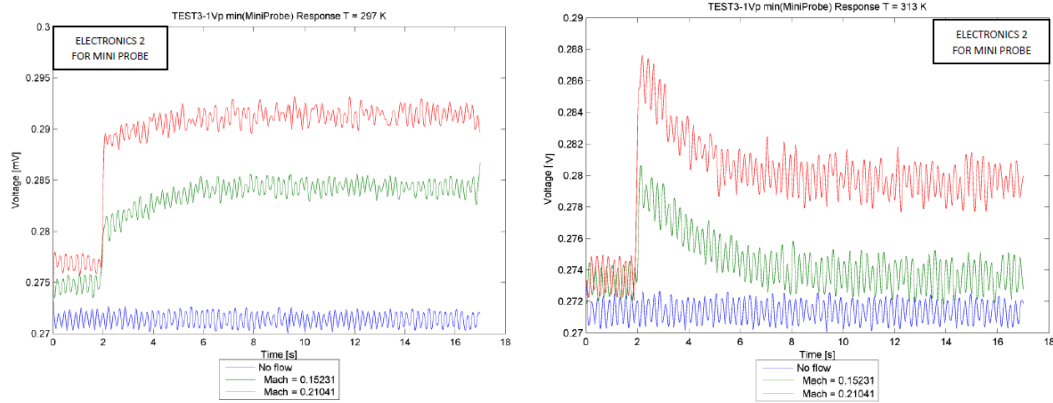


Figure 2.8: Step and stability test for a passive temperature compensated FRAP for flow at temperature of: 297 K (left) and 313K (right) (García 2014)

Even with the compensation module, probe's voltage signal isn't comparable for equal Mach number flows if they occur at different temperature values, Figure 2.8.

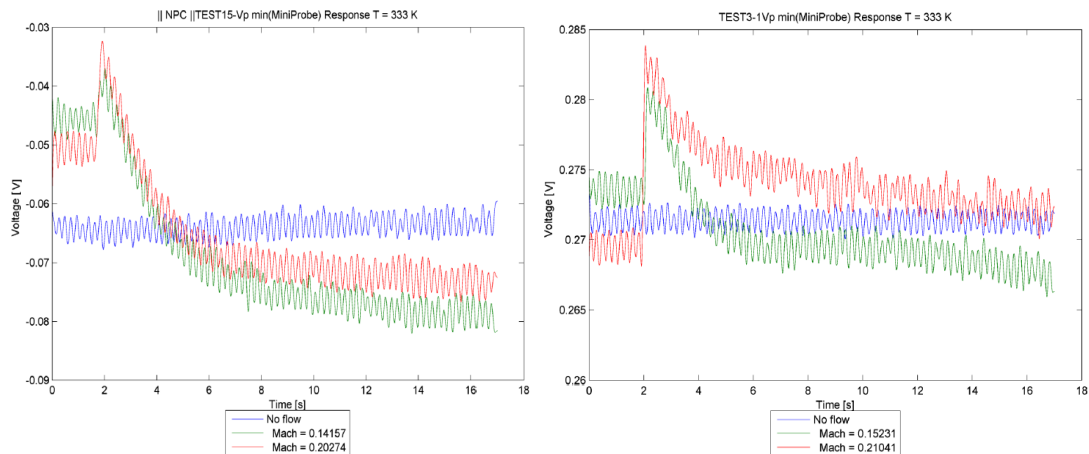


Figure 2.9: Step and stability test for a FRAP: without any temperature compensation (left) and with a passive compensation (right) (García 2014)

As it can be observed also in Figure 2.9, the outcome of this correction only improved slightly the stabilization time and did not at all correct the temperature effect present in these devices; thusly it is not used in the present assignment.

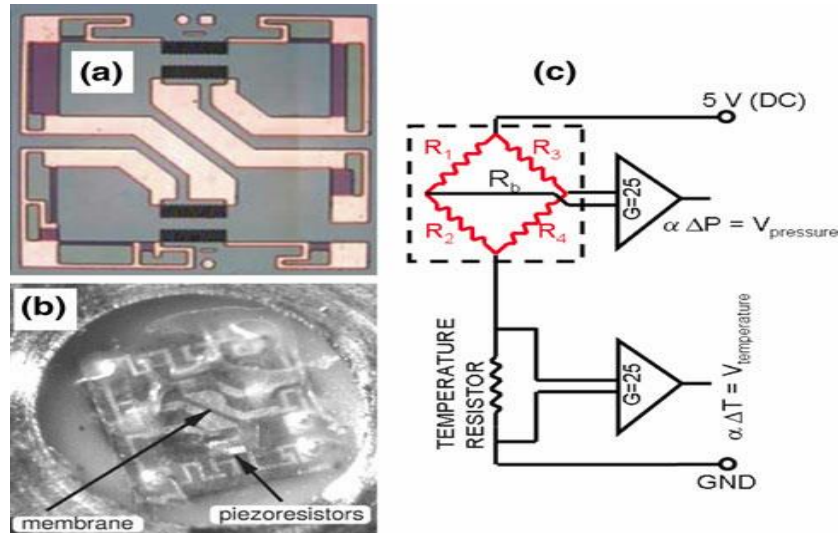


Figure 2.10: (a) bare piezo-resistive gauge picture, (b) implementation of a Kulite® gauge in a Pitot probe with a protective silicon layer and (c) active temperature compensation circuitry (Delhay, Paniagua, et al. 2010)

On the other hand, the principle of active compensation is to take into account the overall bridge resistance, which reflects the sensor's temperature, and to use it to correct the pressure signal output by the bridge. This can be done using more circuitry to modify the bridge output, and/or through post-processing numerical correction. In order to measure the overall resistance of the Wheatstone bridge, the latter is included in a half-bridge, where the temperature sensitivity resistor is used in series with the full bridge illustrated in Figure 2.10.(c). Hence, a change in the resistance of the full bridge i.e. V_{pressure} , hereafter solely mentioned as V_p , will be accurately measured through the change in $V_{\text{temperature}}$, from now on named V_s , measured across the sense resistor.

A post-processing correction will compute this two voltage signals together with a reference pressure in order to obtain an accurate calibration law that allows a fine control of this thermal error and this is explained in detail in (Dénos 2002).

2.5. Fast-Response Pressure Probes

The present work is regarding two different sets of probes designed and built at the VKI. Their design and analysis description can be found in (Bonetti 2013), data processing development is depicted in (Morelli 2014) as well as some preliminary calibrations in (García 2014).

Pressure transducers are built in a flush mounted configuration for both sets of probes. Three probes have Kulite® XCQ-062 series transducers with an external diameter of 2.0 mm and six probes have Measurement Specialties™ EPIH-11 without screen transducer with a smaller diameter of 1.6 mm, both have the same length of 75 mm, Figure 2.11Figure 2.12.

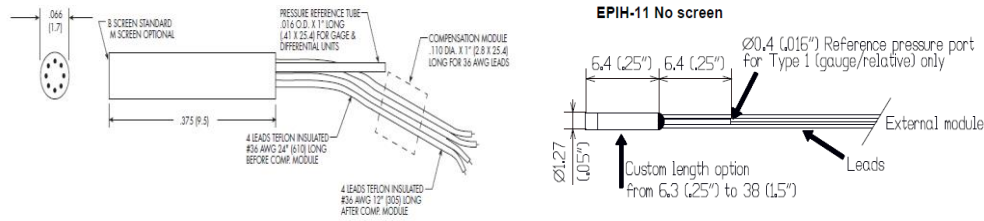


Figure 2.11: Transducers drawings: Kulite® XCQ-062 (left) and Measurement Specialties™ EPIH-11 (right)

The geometry greatly affects the dynamic errors and the circular cylinder was the least affected by dynamic flow phenomena such as dynamic circulation-induced lift, inertia effects, dynamic boundary layers, dynamic stall and vortex interaction, Figure 2.12 (right). In fact, no dynamic stall is found to occur on circular cylinders according to (Gossweiler 1996) and it was reported in (Brouckaert 2014) that this probe's geometry is affected practically only by vortex interactions induced by the Karman vortex street behind the body.

Considering this, probes were designed and manufactured in circular cylinder geometry, as illustrated in Figure 2.12 (left), due to its good behaviour in unsteady flows and also for the space availability inside between stator-rotor stages.

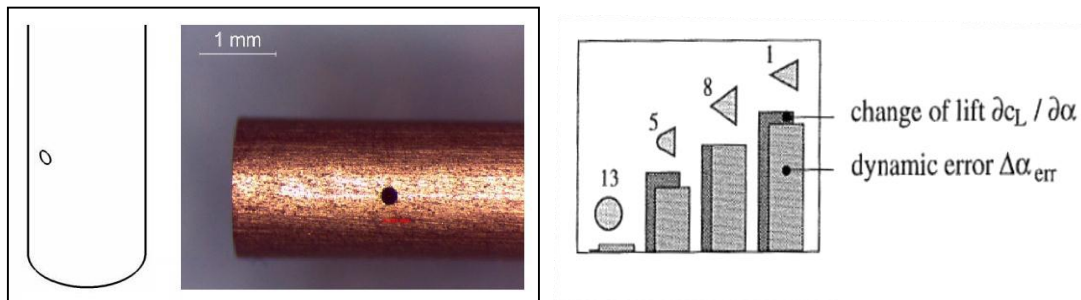


Figure 2.12: Kulite sensor FRAP: illustration and photograph (Bonetti 2013) (left) and comparison of change of lift and dynamic errors for different geometries [Humm 1996] (right)

On Table 2.1, probe nomenclature used in this project is presented along with its respective transducers and dimensions.

<i>FRAP name</i>	<i>Transducer</i>	<i>Diameter [mm]</i>	<i>Length [mm]</i>
DAO129A	EPIH-11	1.6	75.0
DAO129B	EPIH-11	1.6	75.0
DAO129C	EPIH-11	1.6	75.0
DAO129D	EPIH-11	1.6	75.0
DAO129E	EPIH-11	1.6	75.0
DAO129F	EPIH-11	1.6	75.0
DAO132A	XCQ-062	2.0	75.0
DAO132B	XCQ-062	2.0	75.0
DAO132D	XCQ-062	2.0	75.0

Table 2.1: List of pressure probes and dimensions

For the present work, a configuration evaluation is to be performed for the disposition of these fast-response pressure probes in the wind tunnel for two-dimensional flow measurements. As previously mentioned, at least three pressure measurements are required for this purpose. This can be achieved either by using three probes in the facility at different angles, which further increases the blockage effect, or just one probe with different angular positions for each one of three tests. For both these methods, three pressure voltage acquisitions will be afterwards subjected to calibration data-processing described in the following chapters.

According to (Kupferschmied, Koppel, et al. 2000) using only one sensor in a virtual three probe has the following advantages:

- Only one sensor has to be controlled during the measurements.
- Only one amplifier, one A/D converter and fewer electric connections are necessary, reducing the system complexity and the potential for errors.
- Only stochastic measurement errors from one sensor must be considered in the flow quantities.

However, this is a comparison to a probe with three sensors, different from a single sensor probe, which, to be used for two-dimensional flows, would require three tests to record pressure measurements. Thus, errors such as facility's test to test variations and probe angular positioning errors have also to be considered.

3 FRAP Static and Angular Calibration

Data Post-Processing

3.1. Static Calibration

The sensor's response to the pressure fluctuations is in the form of a voltage signal which can be described mathematically by a linear regression, a polynomial fit or a logarithmic shape, among others. Such calibration law depends on the device's working principle and proprieties which, in this case, matches a multiple linear regression with two variables, pressure voltage and temperature sensitivity voltage.

However, the static calibration used in the angular calibration does not take into account the temperature sensitivity voltage, since it was made under ambient conditions and the jet flow has low temperature, thermal effect was considered small enough to be neglected. This calibration process is described in section 3.1.1.

Regardless, the target pressure measurements will take place in a high temperature environment, and consequently, a different calibration to provide temperature compensation will be required. The procedure to obtain the calibration coefficients for the two sensor signals is to this date still in progress; nevertheless it will be explained in detail in section 3.1.2.

3.1.1. Static Pressure Indicator Calibration

The purpose of this calibration is to acquire linear regression coefficients to convert the voltage signals into pressure values to be afterwards used in the angular calibration.

Very small variations in the temperature sensitivity voltage were observed and since the angular calibration facility is also under the same ambient conditions, the thermal effect was disregarded and thusly, only the pressure voltage signal was used for the calibration.

Static calibration of pressure probes was performed in a differential pressure indicator and the calibration law was obtained through a linear regression of ten values of pressure and voltage using two coefficients, presented in Table 3.1 along with the respective coefficients of determination.

<i>Probe</i>	<i>B</i>	<i>D</i>	<i>R²</i>
DAO129A	0.9550	0.0612	0.999976
DAO129B	1.0853	0.1158	0.999997
DAO129C	0.9080	-0.2142	0.999963
DAO129D	1.2368	0.1425	0.999994
DAO129E	0.9760	0.0913	0.999984
DAO129F	0.7842	0.1643	0.999995
DAO132A	1.0015	0.1761	0.999997
DAO132B	0.6549	0.1529	0.999999
DAO132D	0.8644	0.1667	0.999999

Table 3.1: FRAP's initial static calibration coefficients

3.1.2. In-situ Calibration

Calibration in-situ is able to reduce significantly offset and gain errors (Kupferschmied, Gossweiler and Gyarmathy 1994) due to similarity to test conditions.

This calibration process to be held in the available turbine test rig is fully described in (Dénos 2002) as well as thermal and rotation influence on fast-response pressure transducers in this facility.

CT-3 Facility and Test Conditions

This facility is a short duration wind tunnel for aero-thermal testing of engine-size annular rotating turbine stages in aero-engine similarity. Experiments are performed to characterize the transonic flow in a high pressure turbine stage (Lavagnoli 2012).

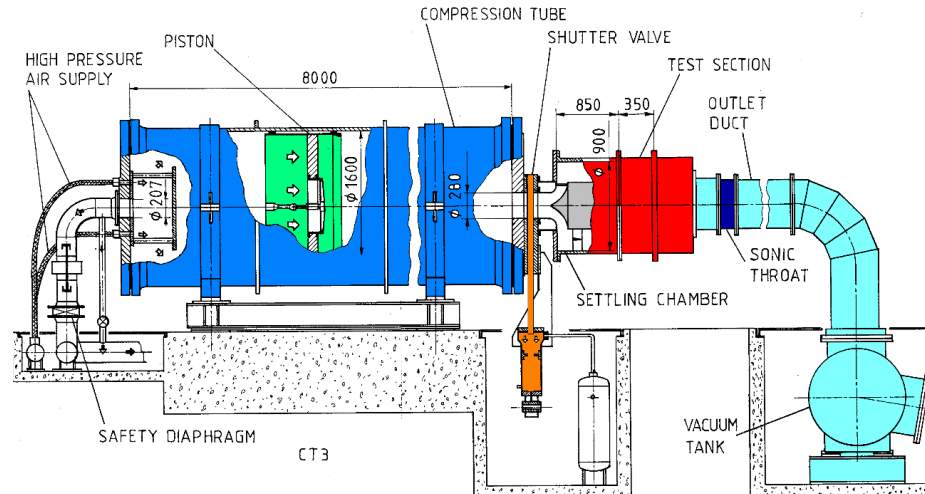


Figure 3.1: Lateral view of CT-3 (Lavagnoli 2012)

The facility's test section contains a $1\frac{1}{2}$ stage turbine and is located between two reservoirs: the upstream compression cylinder and the downstream dump tank. Upon performing a test, the shutter valve is at first closed, isolating the test section from the upstream cylindrical reservoir. The test section is initially at ambient conditions. In order to begin a test, vacuum is set in the dump tank and the turbine rotor is spun up to almost its design speed, which is called the *run-up* phase. High pressure air is admitted in the back of the upstream cylinder. The piston then compresses the air inside the cylinder and, once it reaches the desired pressure, the fast opening shutter valve is opened. A blowdown of hot gas in the test section simulates this way heat transfer to the turbine's blades and endwalls (Paniagua 2002).

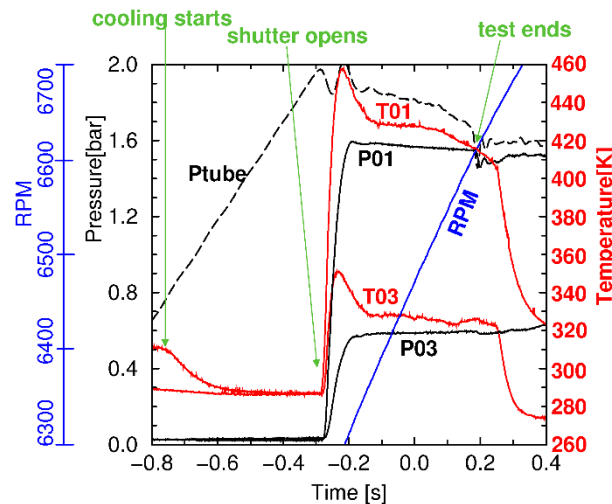


Figure 3.2: Typical test conditions in the CT-3 (Lavagnoli 2012)

Considering the test conditions on which the probes will be performing pressure measurements on Figure 3.2, a calibration law with four coefficients becomes necessary to account for the high temperature variations during the short course of a test. Hence, a new calibration is required to account for the temperature sensitivity voltage signal and also to

set the probes for pressure and temperature transient conditions, which will occur during the turbine testing blow-down.

Run-Up/Run-Down

The process in which temperature and pressure transients are simulated for in-situ calibration is named *run-up/run-down*, shifting from vacuum to ambient conditions. It commences with the chamber sealed and depressurized to approximately 50 mbar and the rotor is put into rotation until it reaches around 6000 rpm. During the rotor's spin up, the ventilation losses increase and as a consequence the sensor's temperature increase as well, inducing the intended temperature transient. On reaching the target rotor speed, the air supply of the aero-brake is opened and air is released in the test section, rapidly increasing the pressure and temperature due to the compression in a closed volume. Subsequently, the test section is opened to the atmosphere nonetheless, due to the continuous admission of cold air from the brake, the test section stays slightly above atmospheric pressure and the sensor temperature starts to decrease. At 630 s since the beginning of this calibration, the brake is finally stopped and the pressure in the test section returns to the atmospheric pressure; the temperature continues to decrease (Dénos 2002).

Figure 3.3 presents both the rotational speed evolution and the pressure comparison between the fast-response and the reference pneumatic probes and Figure y displays the transducers temperature during the calibration.

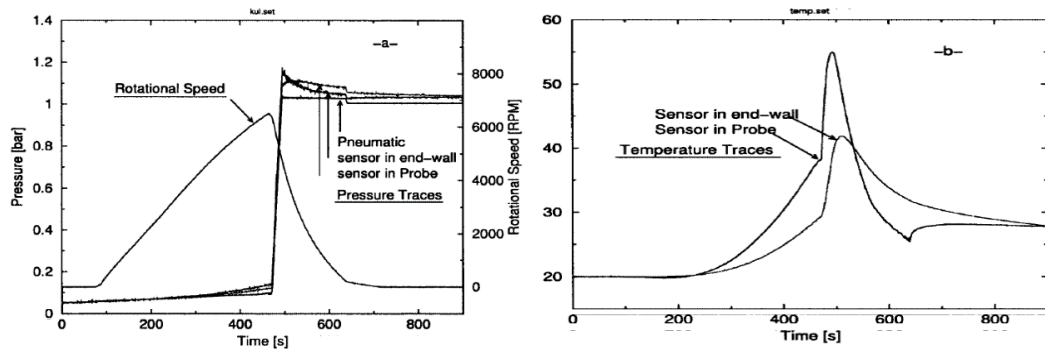


Figure 3.3: Pressure and rotational speed (left) and temperature (right) during in-situ calibration (Dénos 2002)

During the whole process, the readings of the sensors are recorded. The calibration coefficients are then found by fitting the curves to the dump tank pressure, which is measured using a (slow-response) transducer insensitive to temperature. This is performed using a Matlab® script named *find_coefficients* which minimizes the sum of the absolute differences between the reference pneumatic probe pressure values and the multiple linear regression calibration law of the FRAP voltage signals as depicted in (3.1), (Delhay 2006).

$$e^2 = (P_{Ref} - [(A \cdot V_s + B) \cdot V_p + C \cdot V_s + D])^2 \quad (3.1)$$

An illustration of this method is available in Figure 3.4.

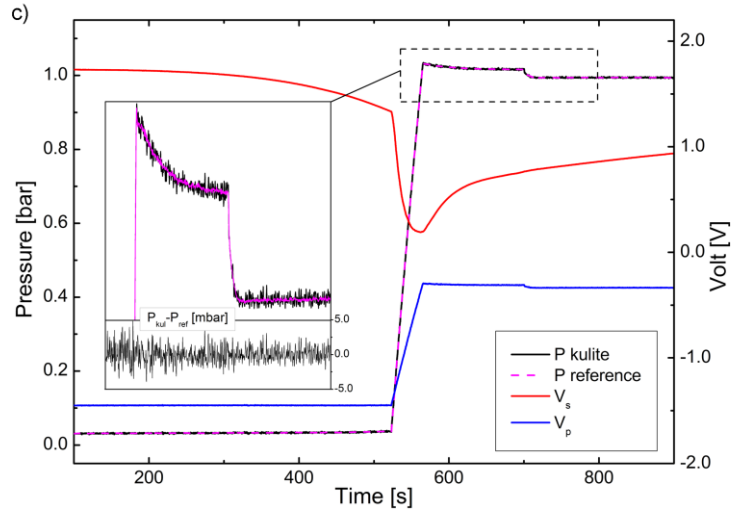


Figure 3.4: In-situ calibration of FRAP voltage signals with reference pneumatic pressure probe (Lavagnoli 2012)

Static Calibration of Transducers for Reference Five-Hole Pneumatic Pressure Probe

A pneumatic five sensor probe requires five pressure taps inside the wind tunnel and also five pressure transducers at the end of each pressure line.

Measurement chain for the static calibration of the five pressure transducers to use in the reference pneumatic probe for in-situ calibration is presented on Figure 3.5.

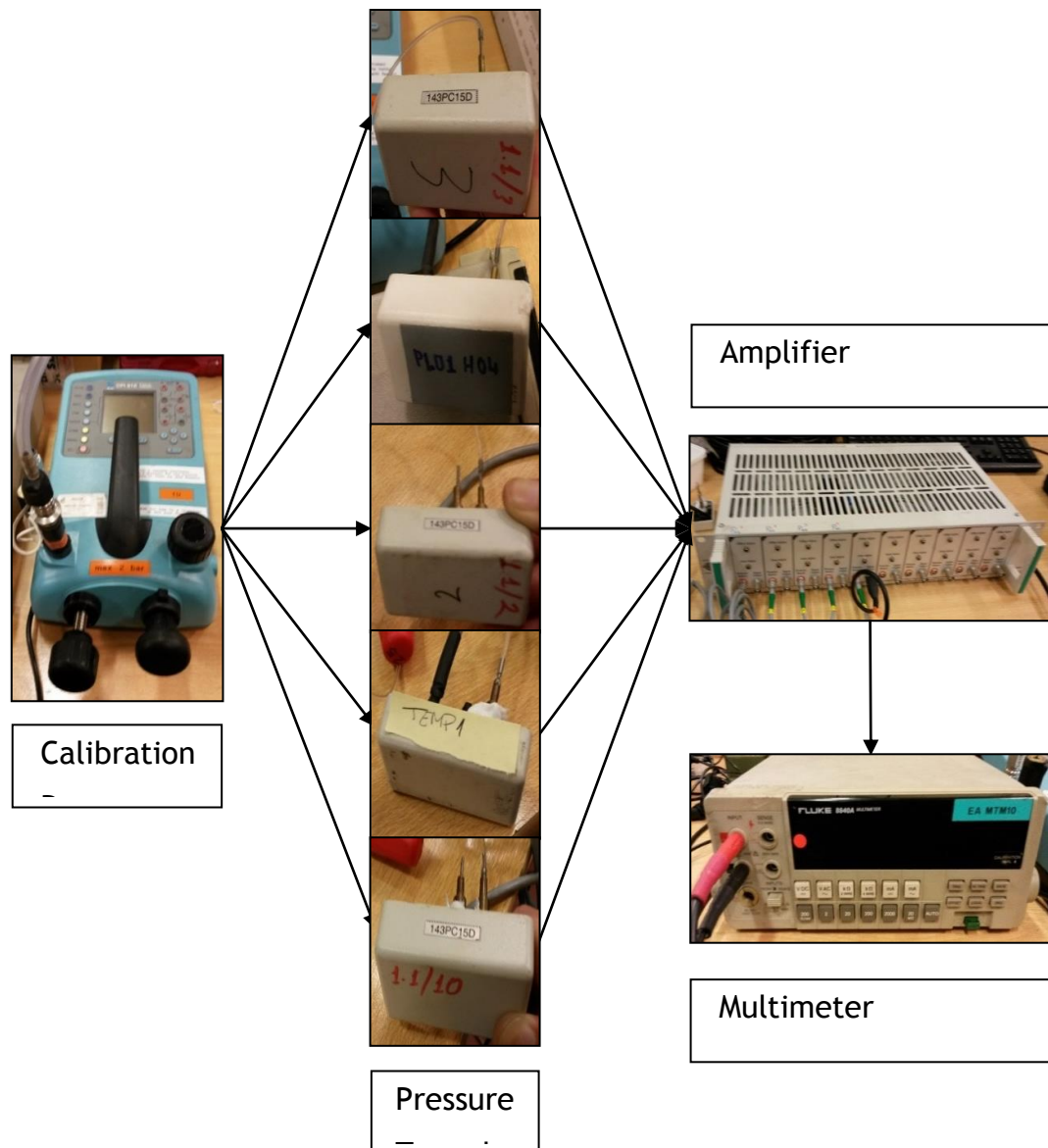


Figure 3.5: Measurement chain of reference pressure transducers

Transducer	143PC15D1.1 3	PL01H04	143PC15D1.1 2	TEMP1	143PC15D1.1 1
Slope	214,1	218,4	216,1	219,7	229,4
Intercept	-0,9426	1,812	-1,023	0,3780	-2,578
R square	0,999997	0,999992	0,999999	0,999990	0,999997

Table 3.2: Static calibration coefficients of reference transducers

3.2. Angular Calibration

Probes aiming to characterize flow direction without recurring to the *equi-balanced* method described in section 1.1 require also a prior calibration. To be precise, an angular calibration to establish relationships between its own pressure values and its angular position in reference to the flow as well as the flow total and static pressure.

Description of this method as well as results is presented in the following sections.

3.2.1. C-4 Facility and Experimental Set Up

Angular calibration of fast response pressure probes is made in the C-4 facility at the VKI, Figure 3.6.

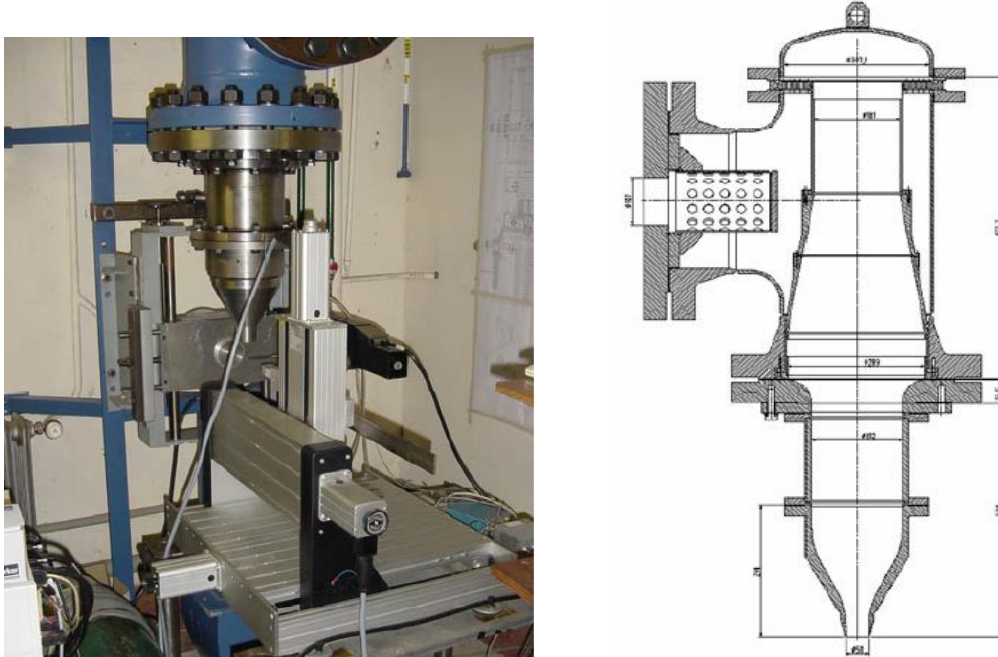


Figure 3.6: C-4 facility: photograph (left) and lateral view drawing (right) (Morelli 2014)

This facility consists on a vertical nozzle to produce constant flow and an electrical linear motor to rotate the probe. The nozzle has a contraction ratio of 14.75 and an outlet diameter of 50 mm and its flow can reach at least a Mach number of 0.8. Considering static pressure as the room atmospheric pressure, which can be assumed constant during the calibration process, the nozzle flow pressure is set accordingly to the targeted Mach number following equation (3.3). The electrical motor is controlled through an ASCII code where measurements sequences are programmed by the user. Probe rotations are made in either the yaw or the pitch direction for each movement.

The accuracy quoted in the angle calibration is better than ± 0.5 deg.

Data acquisition recordings were sampled at 2 kHz following the Nyquist theorem: $f_s > 2f$ to avoid aliasing phenomena (Anthoine, et al. 2009).

In these experiments, the set-up also included a pitot probe completely facing the flow in order to provide reference total pressure and RTD devices to acquire room temperature throughout the calibration procedure.

3.2.2. Yaw and Pitch Angle Measurement Sequences

To achieve a full characterization of the flow present in the wind tunnel, calibration should be made over a wide range Mach number, yaw and pitch angle. In the current assignment, pitch angle will not be used in the calibration and therefore, it is not going to be part of the flow reconstruction. Nevertheless, it was a variable during the process for an subsequent evaluation of its influence in retrieving the flow quantities.

The present calibration was made at two different measurement sequences, one which rotates the probe only in yaw direction in steps of 2° and the other varies both yaw and pitch angle by a 5° angle step. In both sequences the yaw angle is evaluated from -80° to $+80^\circ$ whereas on the latter the pitch angle is only from -30° to $+30^\circ$.

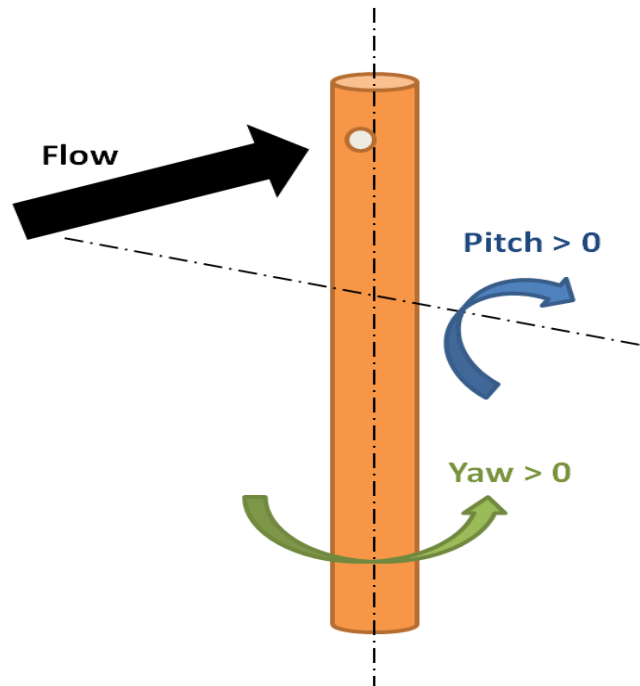


Figure 3.7: Angular calibration reference yaw and pitch angle

3.2.3. Flow Calibration Range

Since calibrations were performed at Mach number above 0.3, the compressibility effect has to be taken into account. Thus,

$$M = \sqrt{\left(\left(\frac{p_o}{p_s} \right)^{\frac{\gamma-1}{\gamma}} - 1 \right) \cdot \left(\frac{2}{\gamma-1} \right)} \quad (3.2)$$

Pitot pressure probe measures total pressure and assuming the atmospheric pressure as the static pressure, Mach number is computed from this pressure measurements.

$$M = \sqrt{\left(\left(\frac{p_{nozzle}}{p_{atm}} \right)^{\frac{\gamma-1}{\gamma}} - 1 \right) \cdot \left(\frac{2}{\gamma-1} \right)} \quad (3.3)$$

Temperature is the average value of four resistance temperature detectors measurement data.

Since the speed of sound is:

$$a = \frac{M}{U} = \sqrt{\gamma RT} \quad (3.4)$$

Through speed of sound definition, velocity is:

$$U = M \sqrt{\gamma RT} \quad (3.5)$$

For the viscosity of the flow, Sutherland formula is used:

$$\mu = \mu_{ref} \left(\frac{T_{ref} + C}{T + C} \right) \left(\frac{T}{T_{ref}} \right)^{\frac{3}{2}} \quad (3.6)$$

Using perfect gas equation, volumetric mass:

$$\rho = \frac{p_{atm}}{RT} \quad (3.7)$$

Finally, Reynolds number, where the probe's diameter is the characteristic length:

$$Re = \frac{\rho U D}{\mu} \quad (3.8)$$

To quantify the amount of nozzle flow is recovered by the probe; the following recovery factor was used:

$$\text{Recovery factor} = \frac{P_{FRAP}}{P_{nozzle}} \quad (3.9)$$

Flow calibration range for every probe is listed on Table 3.3. Overall Mach number range is at least between 0.13 and 0.55 with the exception of probe DAO132B.

<i>Probe</i>	<i>Mach number Range [-]</i>	<i>Reynolds number Range [-]</i>	<i>Vortex frequency Range [Hz]</i>
DAO129A	0 - 0.5648	0 - 20980	0 - 25090
DAO129B	0.0210 - 0.5596	767.1 - 20760	938.6 - 24870
DAO129C	0.1325 - 0.5684	4797 - 20950	5912 - 25180
DAO129D	0.1355 - 0.5540	4883 - 20410	6055 - 24540
DAO129E	0.1437 - 0.5776	5116 - 20830	6445 - 25780
DAO129F	0.1389 - 0.5950	4965 - 21980	6222 - 26330
DAO132A	0.1377 - 0.5950	6150 - 27240	4937 - 21140
DAO132B	0.1367 - 0.4665	6138 - 31180	4890 - 16630
DAO132D	0.1343 - 0.6010	6018 - 27450	4809 - 21370

Table 3.3: Flow calibration range

A more detailed list of every angular calibration performed to each probe is presented on Table 3.4 specifying also yaw and pitch angle range.

<i>Test Name</i>	<i>M</i>	<i>Re</i>	<i>Yaw angle [°]</i>		<i>Pitch angle [°]</i>		<i>P_{amb}</i> [bar]
	[-]	[-]	<i>Range</i>	<i>Step</i>	<i>Range</i>	<i>Step</i>	
DAO129Abis001	0.1736	0	± 80	2	0	–	1.009
DAO129Abis002	0.2725	7261	± 80	2	0	–	1.009
DAO129Abis003	0.3881	12580	± 80	2	0	–	1.009
DAO129Abis004	0.3881	12300	± 80	5	±30	5	1.009
DAO129Abis005	0.4884	16760	± 80	2	0	–	1.009
DAO129Abis006	0.6029	20980	± 80	2	0	–	1.009
DAO129Bbis001	0.0210	767	± 80	2	0	–	1.008
DAO129Bbis002	0.2011	7386	± 80	2	0	–	1.008
DAO129Bbis003	0.3397	12550	± 80	2	0	–	1.008
DAO129Bbis004	0.4582	16980	± 80	2	0	–	1.008
DAO129Bbis005	0.5596	20760	± 80	2	0	–	1.008
DAO129C001	0.1325	4797	± 80	2	0	–	0.9928
DAO129C002	0.2376	8662	± 80	2	0	–	0.9928
DAO129C003	0.3581	13140	± 80	2	0	–	0.9928
DAO129C004	0.4567	16810	± 80	2	0	–	0.9928
DAO129C005	0.5684	20950	± 80	2	0	–	0.9928
DAO129D001	0.1355	4883	± 80	2	0	–	0.9933
DAO129D002	0.1429	5187	± 80	5	±30	5	0.9933
DAO129D003	0.2370	8655	± 80	2	0	–	0.9933
DAO129D004	0.3681	13510	± 80	2	0	–	0.9933
DAO129D005	0.3659	13480	± 80	5	±30	5	0.9933
DAO129D006	0.4744	17490	± 80	2	0	–	0.9933
DAO129D007	0.5539	20410	± 80	2	0	–	0.9933
DAO129D008	0.5398	19830	± 80	5	±30	5	0.9933
DAO129E001	0.1437	5116.0	± 80	2	0	–	0.9905
DAO129E002	0.2488	8892.0	± 80	2	0	–	0.9905
DAO129E003	0.3664	13160	± 80	2	0	–	0.9905
DAO129E004	0.4690	16890	± 80	2	0	–	0.9905
DAO129E005	0.5776	20830	± 80	2	0	–	0.9905
DAO129F001	0.1389	4965.0	± 80	2	0	–	0.9924
DAO129F002	0.2484	8976.0	± 80	2	0	–	0.9924
DAO129F003	0.3670	13390	± 80	2	0	–	0.9924
DAO129F004	0.4720	17350	± 80	2	0	–	0.9924
DAO129F005	0.5950	21980	± 80	2	0	–	0.9924
DAO132A001	0.1377	6150	± 80	2	0	–	0.9935
DAO132A002	0.2516	11350	± 80	2	0	–	0.9935
DAO132A003	0.3743	17010	± 80	2	0	–	0.9935

DAO132A004	0.4779	21820	± 80	2	0	–	0.9935
DAO132A005	0.5949	27240	± 80	2	0	–	0.9935
DAO132B001	0.1367	6138	± 80	2	0	–	0.9934
DAO132B002	0.2393	10800	± 80	2	0	–	0.9934
DAO132B003	0.3566	16180	± 80	2	0	–	0.9934
DAO132B004	0.3562	16180	± 80	5	± 30	5	0.9934
DAO132B005	0.4665	21180	± 80	2	0	–	0.9934
DAO132D001	0.1343	6018	± 80	2	0	–	0.9935
DAO132D002	0.2488	11220	± 80	2	0	–	0.9935
DAO132D003	0.3712	16870	± 80	2	0	–	0.9935
DAO132D004	0.4797	21890	± 80	2	0	–	0.9935
DAO132D005	0.6009	27450	± 80	2	0	–	0.9935

Table 3.4: List of angular calibration tests

3.2.4. Calibration Data Post-Processing

A Matlab[®] script is developed to process the calibration data described in the previous sections. Voltage signals along with measurement sequences from the angular calibration at the C-4 and coefficients from the differential pressure indicator static calibration are analysed and processed to generate calibrated pressures values matching known flow quantities: yaw angle, pitch angle, total pressure and static pressure.

These results will allow aerodynamic calibration for the range of the cited flow quantities as well as the analysis of other flow characteristics, such as temperature, Reynolds number and Mach number.

This script operates in two consecutive modes: on the first, coefficients from section 3.1.1 are used for the static calibration and a correlation of peak pressure and voltage value from each test is performed to gather new static calibration coefficients to apply on the second mode. On this last mode, a correction of angle deviation and a frequency analysis of FRAP's voltage signal are also implemented.

Signal Acquisition

Yaw sequence calibrations consist in a forward sweep from -80° to $+80^\circ$ in steps of 2° angles followed by a backwards sweep of a 10° step. At the beginning and end of each sweep a reference point is acquired at null yaw angle. The pitch angle is kept null during the whole calibration.

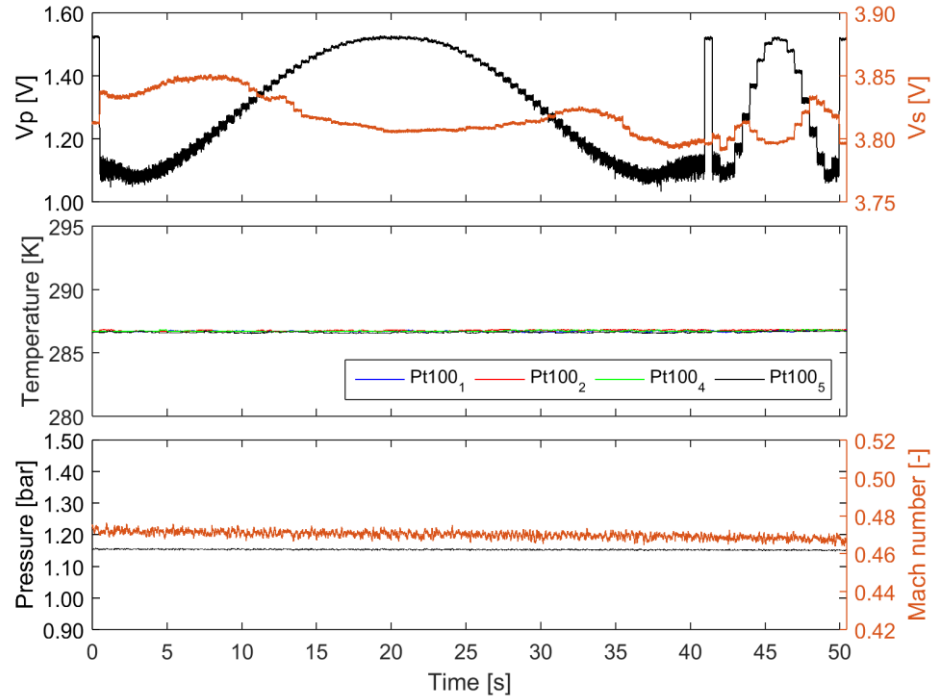


Figure 3.8: FRAP voltage signals, temperature and pressure during yaw angle calibration

Figure 3.8 provides an overview of the calibration flow reference pressure and temperature and also of the fast response probe signal acquisition.

Pressure voltage signal V_p is plotted along with temperature sensitivity voltage signal V_s in the first figure in order to evaluate its influence. It can be observed that V_s overall variation is very small with the exception of when the transducer is completely facing the flow, which has a temperature lower than the room temperature, a lower voltage is therefore recorded.

The other two figures below display the flow temperature, pressure and Mach number. Signals are presented already calibrated in order to verify if calibration flow conditions were within the targeted values.

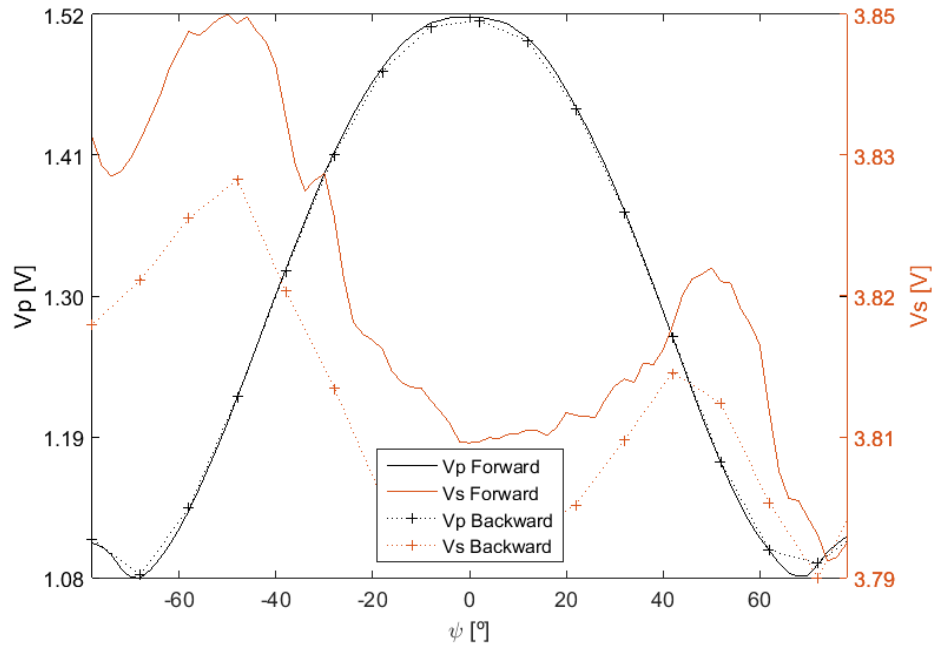


Figure 3.9: Pressure and temperature sensitivity voltage signals

On Figure 3.9 probe's acquired voltage signals V_p and V_s is shown in function of yaw angle for both forward and backward calibration sweep. Repeatability of the pressure signal is verified as well as a negligible variation of temperature sensitivity signal.

Static Calibration Coefficients with Null Angle Total Recovery Assumption

Since the temperature effect for this calibration is almost negligible, calibration only took into account the pressure signal V_p .

Initially, for the first iteration, the script uses the coefficients from a static calibration presented in section 3.1.1, in which no flow is present.

Since transducers are to measure unsteady flow, a calibration sensing not only static but also dynamic pressure is preferred.

To solve this, for each probe, at null pitch angle, the maximum acquired pressure voltage is extracted for every test, closer to a null yaw angle for smaller deviation angles. Then, a linear regression of these values and the flow reference pressure for that acquisition provides new calibration coefficients, Figure 3.10.

In spite of being under a total recovery assumption and also of being less accurate in terms of a lower coefficient of determination, these coefficients are better suited for flow measurements.

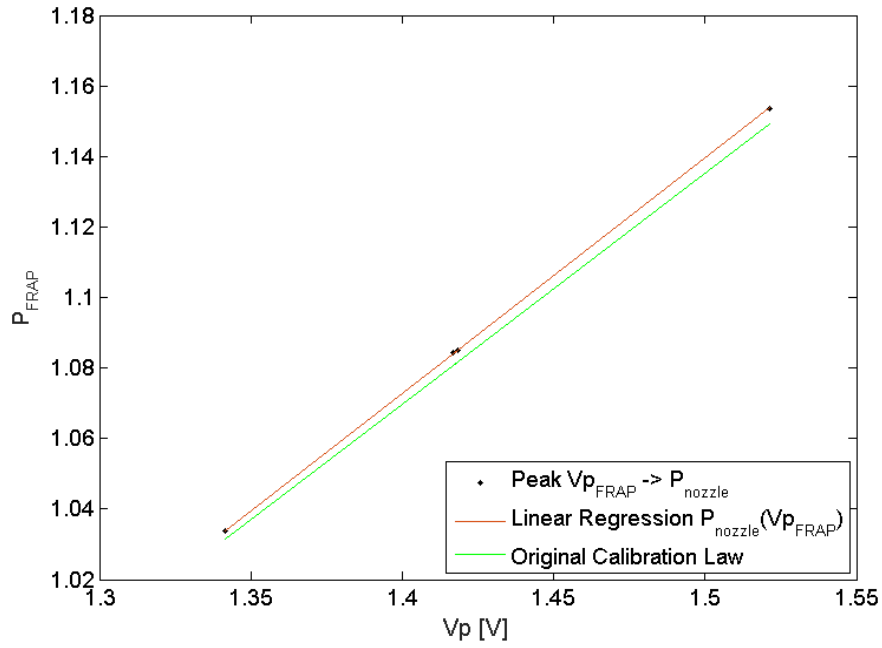


Figure 3.10: New FRAP's static calibration coefficients

Probe	B'	D'	R^2
DAO129A	0.8838	0.1042	0.99961530
DAO129B	1.0956	0.1673	0.99983169
DAO129C	0.9033	-0.1714	0.99994886
DAO129D	1.3088	0.1001	0.99983572
DAO129E	0.9073	0.1264	0.99998945
DAO129F	0.7427	0.1747	0.99961871
DAO132A	1.0165	0.1605	0.99998301
DAO132B	0.6674	0.1384	0.99998624
DAO132D	0.8738	0.1514	0.99997916

Table 3.5: New static calibration coefficients

On obtaining the new static calibration coefficients for each probe presented in Table 3.5, the second and last iteration is performed.

Shift Angle Correction

After the recalibration, a ten degree polynomial interpolation of the probe pressure is used to find the highest pressure value, for, due to manufacturing errors and/or probe mispositioning during the calibration process; the yaw angle considered may not be the true one. This shift in yaw angle is corrected afterwards and the lateral separation angle is computed.

On the first running mode of the script, the deviation angle is computed by simply finding the angle where the peak pressure was acquired, and it is presented on Table 3.6 for each probe along with angles where the flow separation occurs. These values are the average for every calibration test performed to each probe in which their variation is around 3°.

Probe	Left separation angle [°]	Right separation angle [°]	Zero angle shift [°]
DAO129A	-71.0	68.0	-7.0
DAO129B	-71.6	72.8	-5.8
DAO129C	-71.6	71.8	-0.6
DAO129D	-71.1	72.1	-6.0
DAO129E	-70.6	71.8	-8.2
DAO129F	-71.2	71.0	-7.4
DAO132A	-70.6	69.8	-4.8
DAO132B	-70.6	69.4	-2.0
DAO132D	-70.2	69.8	-0.2

Table 3.6: Shift and separation averaged angles

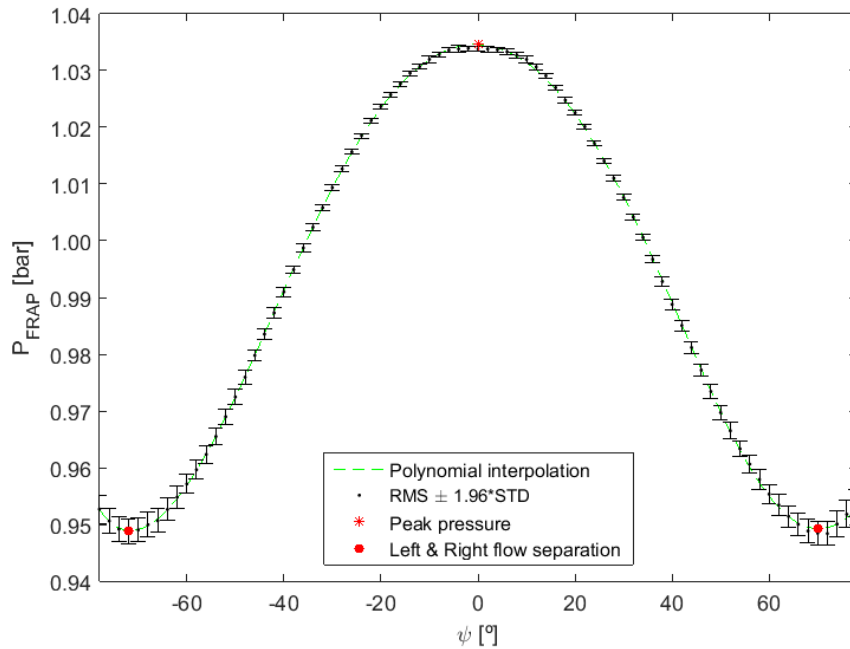


Figure 3.11: FRAP measured pressure for yaw angle

Once the final static calibration coefficients were computed and the angle deviation corrected, the pressure curves in function of yaw angle are obtained for every calibration test of each probe.

Exemplifying this on Figure 3.11, black bars indicate the values in which the signal varied during its acquisition. It can be seen the near the separation point the variation is rather high.

During separation, pressure is constant in every direction and it is insensitive to flow direction.

Analysis of Pitch Fine Sequence

Every calibration test is analysed, whether it matches a yaw or a pitch sequence. However, pitch sequences have additional information to provide, namely, the pitch angle effect on the pressure recovery.

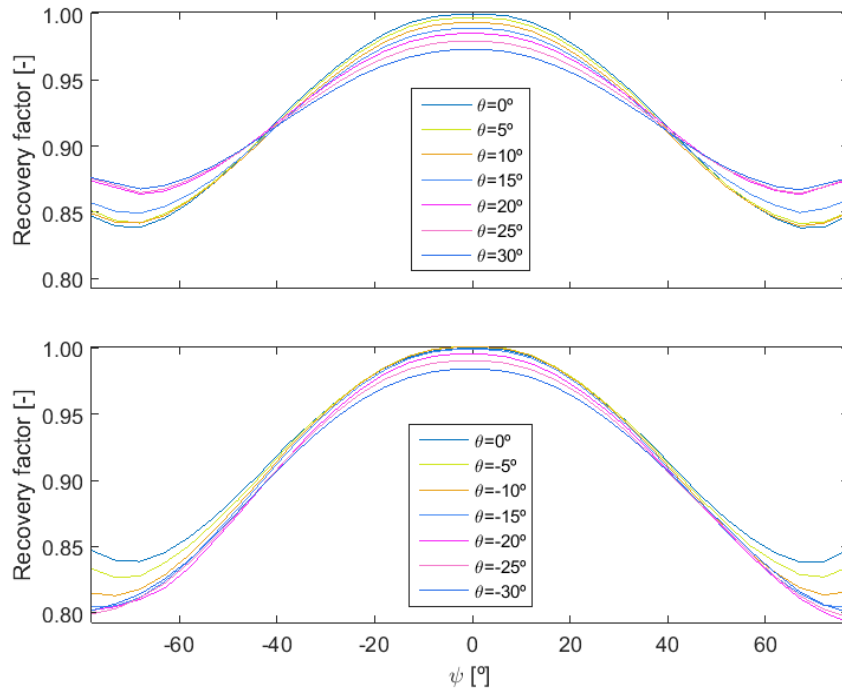


Figure 3.12: Pitch angle influence in flow recovery

Recovery factor for positive and negative pitch angle is presented separately for a better understanding of its variation. It can be observed on Figure 3.12 a lower recovery for the positive pitch angles. This is mostly due to the probe geometry.

Some probes had a higher than one recovery factor at low Mach number. Literature refers to this as the Barker effect: viscous interaction between probe's free stream and stagnation fluid results in an energy transfer and as a consequence in a pressure measurement which is too high (Anthoine, et al. 2009).

Analysis of Yaw Angle Sequences

The main objective of this process is to gather pressure values linked to flow quantities to be used in aerodynamic calibration described in chapter 0, an example for a probe is illustrated in Figure 3.13. Since this calibration does not account for the pitch angle, only sequences where it is null are used for this purpose.

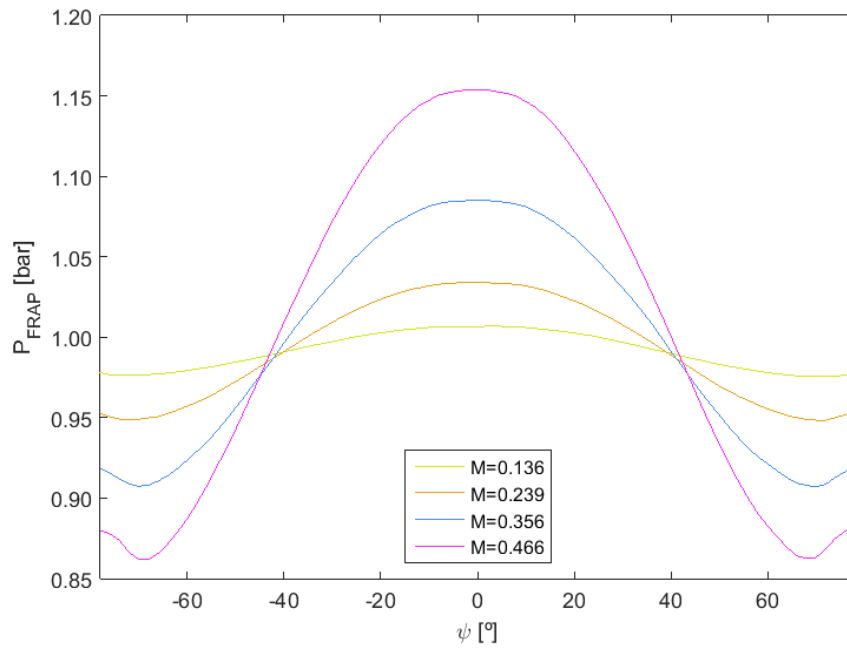


Figure 3.13: Pressure measurements at different Mach numbers

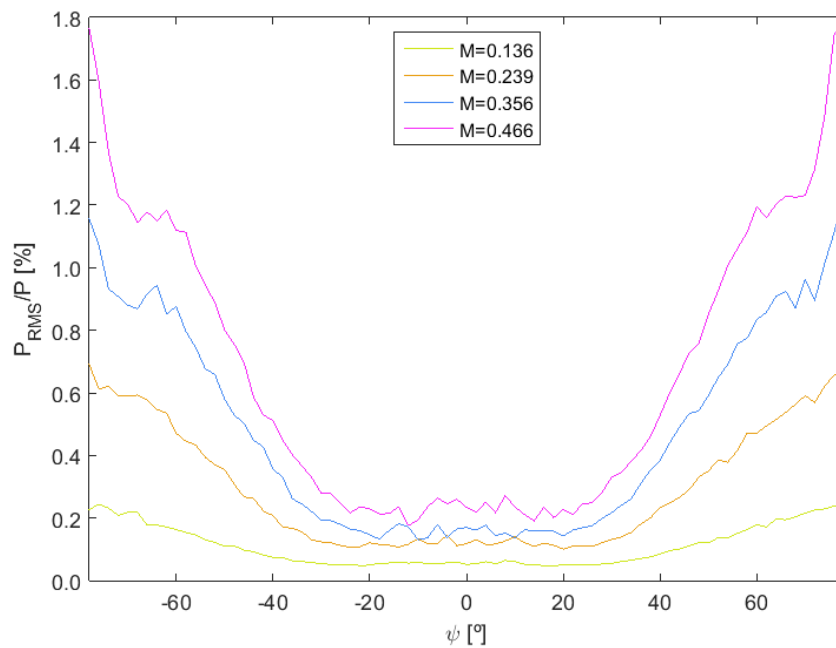


Figure 3.14: Ratio of root-mean-square and mean pressure

As it can be observed in Figure 3.14, pressure signal fluctuations increase with Mach number and, as expected, with angular deviation from the flow.

Every probe equipped with Kulite® sensors demonstrates smaller fluctuations than Measurement Specialties™ sensors.

Moreover, except for a null yaw angle, experimental results present lower fluctuations than those of CFD predictions in (Bonetti 2013).

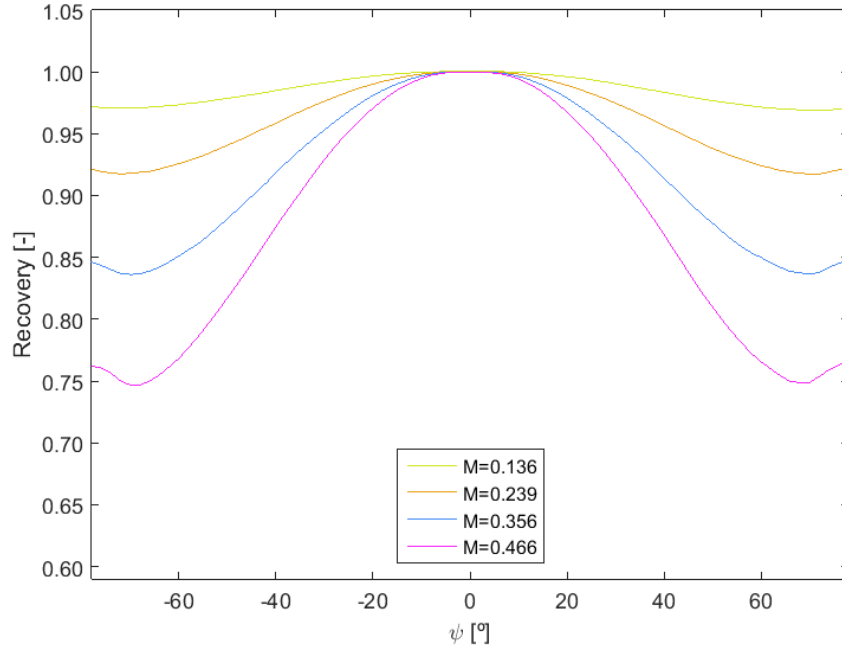


Figure 3.15: FRAP recovery factor of calibration flow

Pressure recovery peak is achieved when the transducer is completely facing the flow. Some effects like the Reynolds number effect, where the viscous interaction between the free stream and stagnation fluid results in an energy transfer and as a consequence, in a pressure measurement too high (Anthoine, et al. 2009), led to a recovery factor higher than one in some probe's acquisitions. As the flow velocity increases, the flow pressure recovery is less efficient, Figure 3.15.

It is verified that angle sensitivity increases with Mach number (Anthoine, et al. 2009).

General Flow Quantities

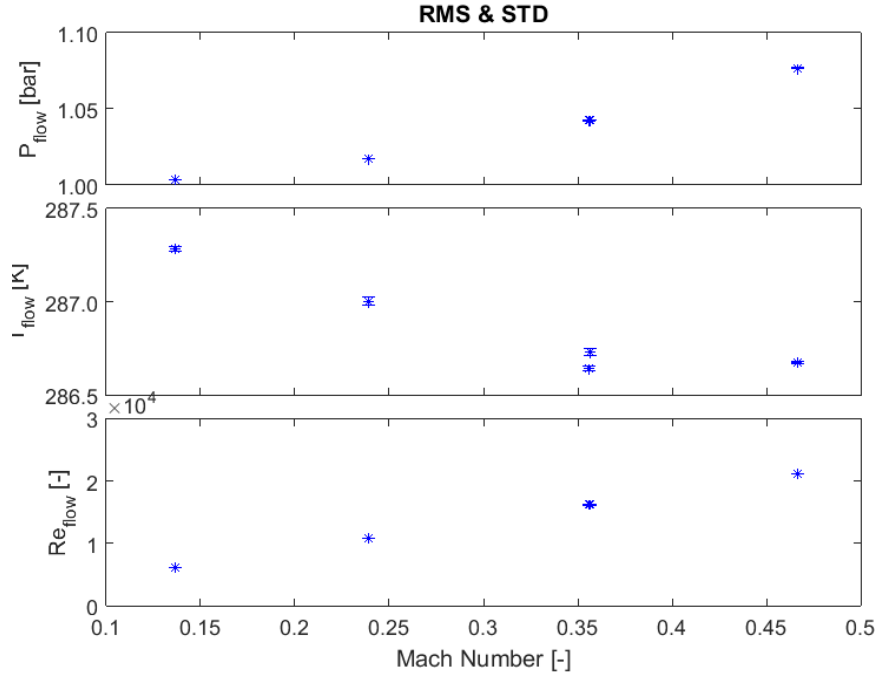


Figure 3.16: Calibration flow pressure, temperature and Reynolds number range

For every probe, information displayed on Figure 3.16 is available to check for each test the temperature, pressure and Reynolds number it was subjected to and if their variation was within acceptable values.

Test	Δp_{nozzle}	p_s	q	F_D	St	M_{targ}	M_{acq}	Re	f_v
	[mbar]	[Pa]	[Pa]	[N]	[-]	[-]	[-]	[-]	[Hz]
1	2.94	99348.25	1325.33	0.19	0.21	0.10	0.14	6150.32	4937.08
2	0.60	99348.25	4471.31	0.64	0.21	0.20	0.25	11344.98	8989.96
3	1.41	99348.25	10088.32	1.44	0.21	0.30	0.37	17012.23	13334.70
4	6.48	99348.25	16810.76	2.40	0.21	0.40	0.48	21816.19	16997.56
5	13.69	99348.25	26873.59	3.83	0.21	0.50	0.59	27241.64	21136.32

Table 3.7: Flow characteristics

Frequency Analysis

Circular cylinders are affected only by vortex interactions induced by the Karman vortex street behind the body (Brouckaert 2014) and resonance phenomena. A signal power spectral density estimate using Welch's method is implemented in terms of pressure instead of voltage since calibration only considers one voltage signal, V_p .

Firstly, the time of each sample acquisition and the sampling frequency is determined:

$$t_{sample} = \frac{\Delta t_{sample}}{N_{samples} - 1} \quad (3.10)$$

$$f_s = \frac{1}{t_{sample}} \quad (3.11)$$

Then, the fluctuating component is computed withdrawing the mean value from the signal:

$$P'_{FRAP} = P_{FRAP} - \overline{P_{FRAP}} \quad (3.12)$$

Finally, spectral density was analysed for every test for a set of angles from -70° to $+70^\circ$ by step of 20° using Matlab® function *pwelch*. Software documentation describes this technique as an overlapping segment averaging estimator to obtain the power spectral density estimate of a signal.

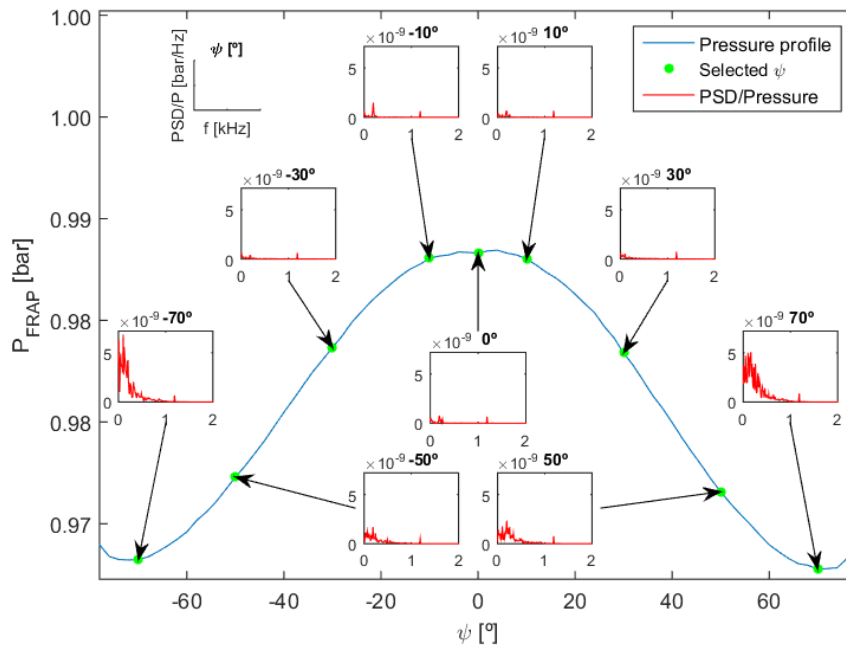


Figure 3.17: Frequency analysis of FRAP's pressure signal

In some tests, at angles between -40° and 40° , power peaks occurred distinctly for 0.2 kHz and/or 1.2 kHz, even though a low pass filter of 1.0 kHz was used for the data acquisition. An example of this is visible on Figure 3.17.

As expected, peaks of power increase with Mach number and occasional occur at a slightly higher frequency.

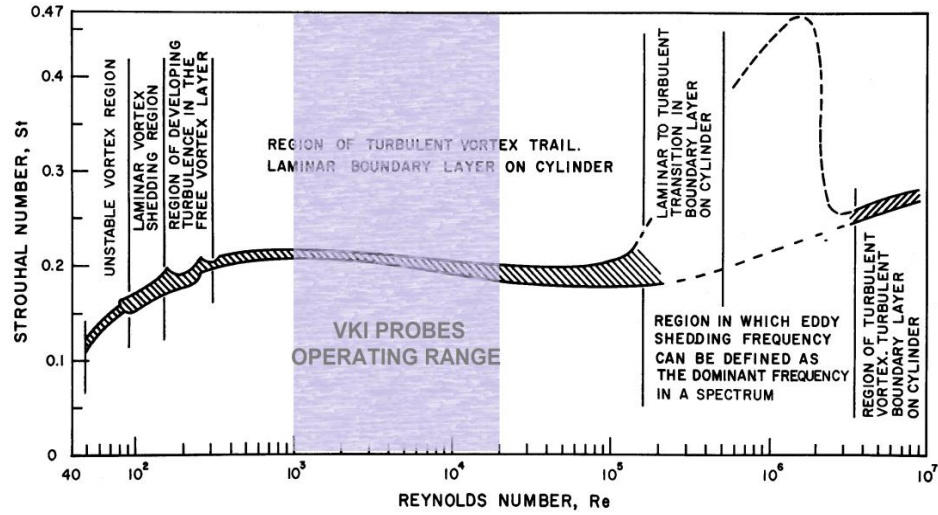


Figure 3.18: Strouhal number for FRAP's Reynolds number operating range (Lienhard 1966)

Expected frequency of vortex shedding is found through Strouhal number, which can be considered constant and approximately equal to 0.21 for the Reynolds number operating range illustrated in Figure 3.18:

$$f_v = \frac{St \cdot V}{D} \quad (3.13)$$

Calibration flow velocities reached a Mach number of 0.6 leading to a maximum vortex shedding frequency of approximately 25 kHz. Unfortunately, sampling frequency for the calibration data acquisition was too low to check for this phenomenon and also for resonance, where predictions during the probe's design in (Bonetti 2013) are always above 40 kHz.

4 FRAP Aerodynamic Calibration

The final step of fast response pressure probes calibration is the computation of aerodynamic calibration coefficients for the flow quantities presented in the Chapter 3.2, i.e. for the probes measured pressure values at a certain angular position, flow velocity and surrounding pressure.

Considering the requirements for 2D flow characterization inside a turbine's wind tunnel, an arrangement of three probes is studied in the following chapters through an aerodynamic calibration script on section 1.1 and uncertainty analysis evaluation on section 1.1.

In sum, after the aerodynamic calibration script optimization, an analysis of the most efficient angle between sensors and central amplification coefficient was conducted as well as an uncertainty analysis of induced pressure error, sensor angle positioning error and pitch angle effect.

4.1. Aerodynamic Calibration Script Description

Three zones calibration coefficients from (Delhay, Paniagua, et al. 2010) are used to build a Matlab® script in (Morelli 2014) to perform the aerodynamic calibration of three time-resolved measured pressures defined by their angular position inside the turbine test rig.

It is worth mentioning that there is a signal error in the right K_{yaw} which was corrected in the script. The final coefficients are as follows:

$$\begin{cases} K_{yaw} = \frac{p_L - p_R}{k_Z \cdot P_C - 0.5 \cdot (p_L + p_R)} \\ K_{Mach} = \frac{0.25 \cdot k_Z \cdot P_C}{k_Z \cdot p_C - 0.5 \cdot (p_L + p_R)} \\ K_{tot} = \frac{p_0 - k_Z \cdot p_C}{k_Z \cdot p_C - 0.5 \cdot (p_L + p_R)} \\ K_{dyn} = 4 - \frac{p_0 - p_s}{k_Z \cdot p_C - 0.5 \cdot (p_L + p_R)} \end{cases} \quad \text{if } k_Z \cdot p_C > p_L, p_R \quad (4.1)$$

$$\begin{cases} K_{yaw} = 4 + \frac{p_R - p_L}{p_L - 0.5 \cdot (k_Z \cdot P_C + p_R)} \\ K_{Mach} = \frac{k_Z \cdot P_C}{k_Z \cdot P_C + p_L - 2 \cdot p_R} \\ K_{tot} = \frac{p_0 - k_Z \cdot p_C}{p_L - 0.5 \cdot (k_Z \cdot P_C + p_R)} \\ K_{dyn} = \frac{p_0 - p_s}{p_L - 0.5 \cdot (k_Z \cdot P_C + p_R)} \end{cases} \quad \text{if } p_L > k_Z \cdot p_C, p_R \quad (4.2)$$

$$\begin{cases} K_{yaw} = -4 + \frac{p_R - p_L}{p_R - 0.5 \cdot (k_Z \cdot P_C + p_L)} \\ K_{Mach} = \frac{k_Z \cdot P_C}{k_Z \cdot P_C + p_R - 2 \cdot p_L} \\ K_{tot} = \frac{p_0 - k_Z \cdot p_C}{p_R - 0.5 \cdot (k_Z \cdot P_C + p_L)} \\ K_{dyn} = \frac{p_0 - p_s}{p_R - 0.5 \cdot (k_Z \cdot P_C + p_L)} \end{cases} \quad \text{if } p_R > k_Z \cdot p_C, p_L \quad (4.3)$$

These three sets of equations each match a zone correspondent to an angular interval where the pressure of one sensor is higher than on the others. The factor k_Z is used to increase the output of the central sensor (Delhay, Paniagua, et al. 2010) and it can be optimized through a linear combination of coefficients, which is later explained in section 4.2.2.

Aerodynamic coefficients are generated for a selected probe arrangement, defined by which sensors the user selects and its angular position relative to the flow direction. Central sensor amplification coefficient k_Z also influences this process.

Pressure values from angular calibration data of selected left, central and right sensors are loaded and arranged accordingly to this established parameters. Each of these pressure values match a yaw angle and Mach number acquisition during the angular calibration on section 3.2, thus defining a range in which the flow can be characterized.

As an example, angular calibration data from FRAP DAO129D are used to further explain the aerodynamic calibration procedure and also its subsequent use to retrieve flow quantities from pressure measurements of unknown flow. This sensor was selected for the sole purpose of an afterwards evaluation of the pitch angle effect, due to fact that it is the only sensor holding more than one pitch sequence calibration.

A relative angular position of 35° between sensors is used and the central amplification coefficient k_Z is equal to 1.002.

As a result, the obtained aerodynamic calibration coefficients for this configuration are shown in Figure 4.1, in function of flow yaw angle and Mach number.

Finally, the calibration process of fast-response pressure probes is at last complete.

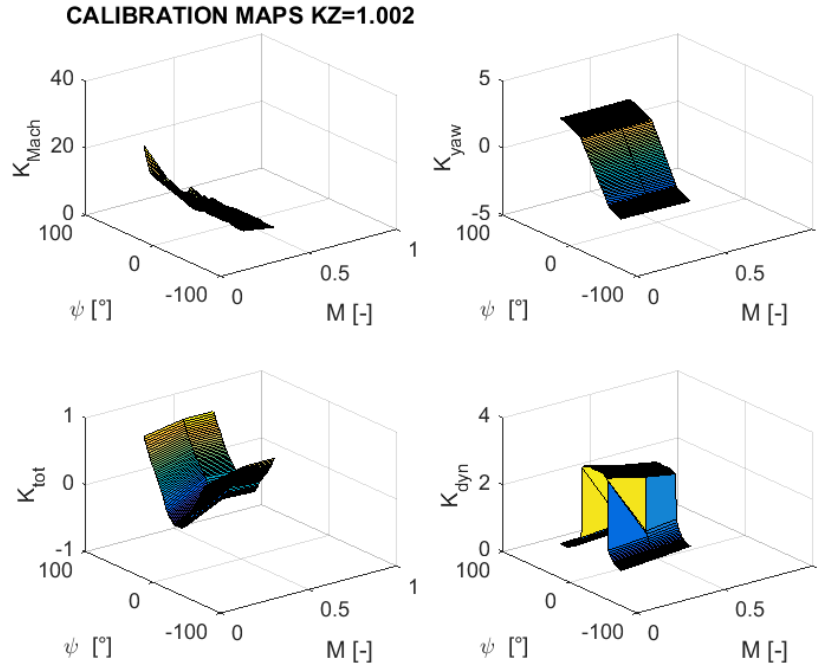


Figure 4.1: 3D maps of aerodynamic calibration coefficients

Flow Quantities Reconstruction

Nonetheless, once the calibration is gathered, a routine inside the script is able to do the reverse procedure, i.e. to evaluate the coefficients for time-resolved measured pressures calibrated as depicted in section 3.1.2.

To achieve this, the same configuration used for the aerodynamic calibration has to be used for the flow reconstruction and the pressure measured for that probe arrangement has to be made available.

Again, this method is exemplified with the probe arrangement used in section 4.1 and a set of pressure measurements, which is described in the following section 4.1.1.

Figure 4.2 displays pressure values taken from correspondent probe angular calibration points used as virtual three-hole probe measurements.

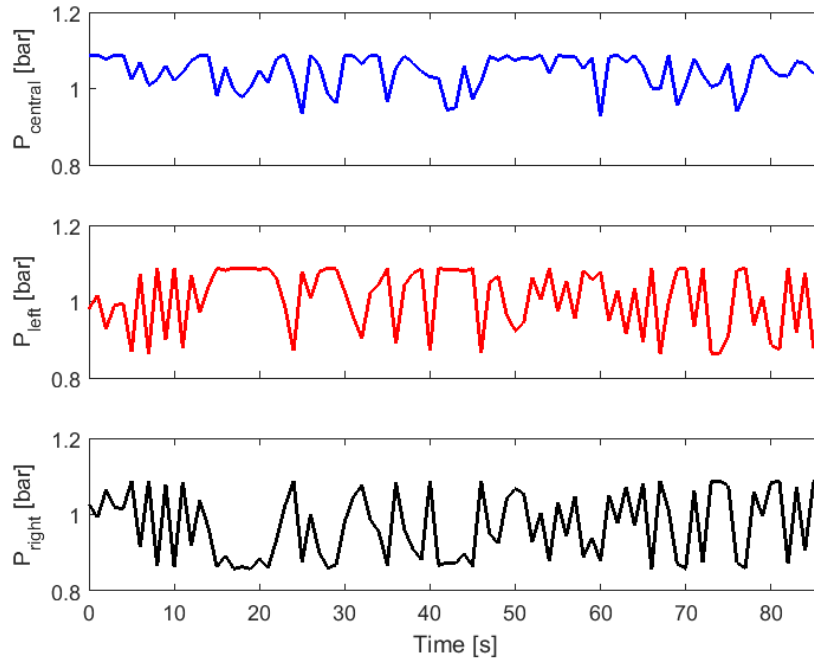


Figure 4.2: Virtual three sensor probe pressure measurements

Each time discrete pressure value is evaluated in the script for flow retrieval, if available within the calibration range. For this purpose, left, central and right sensor pressure values are combined together following the equations (4.1), (4.2) and (4.3) to compute coefficients K_{Mach} and K_{yaw} .

A small routine named *isincell* then finds the cell within the coefficients values linked to a yaw angle and Mach number interval which can be observed in the Figure 4.3. After the cell is determined, it is divided into smaller cells and the same routine is applied. This refinement is set initially by the user.

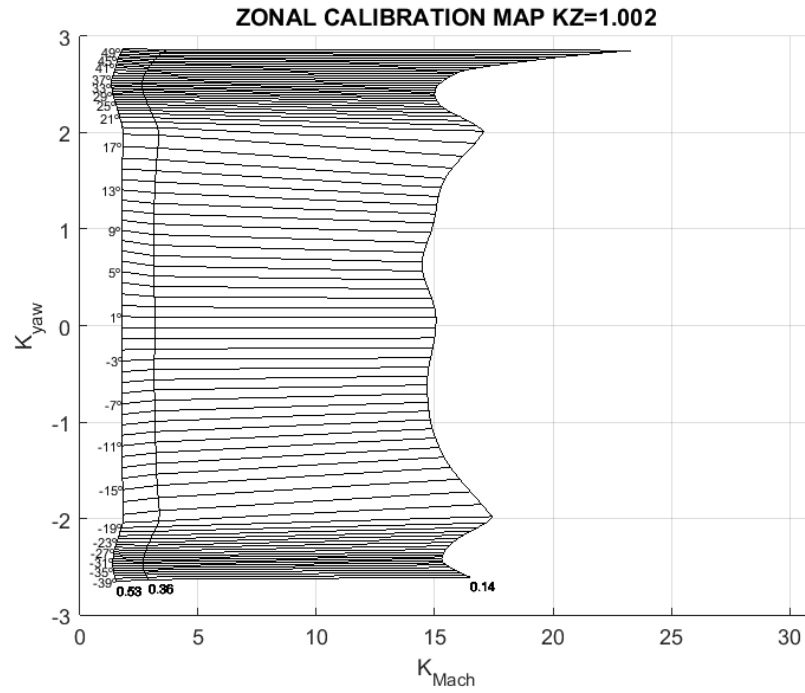


Figure 4.3: Zonal calibration map

Once yaw angle and Mach number are retrieved, they are used in K_{tot} and K_{dyn} coefficients equations to determine the static, dynamic and total pressure.

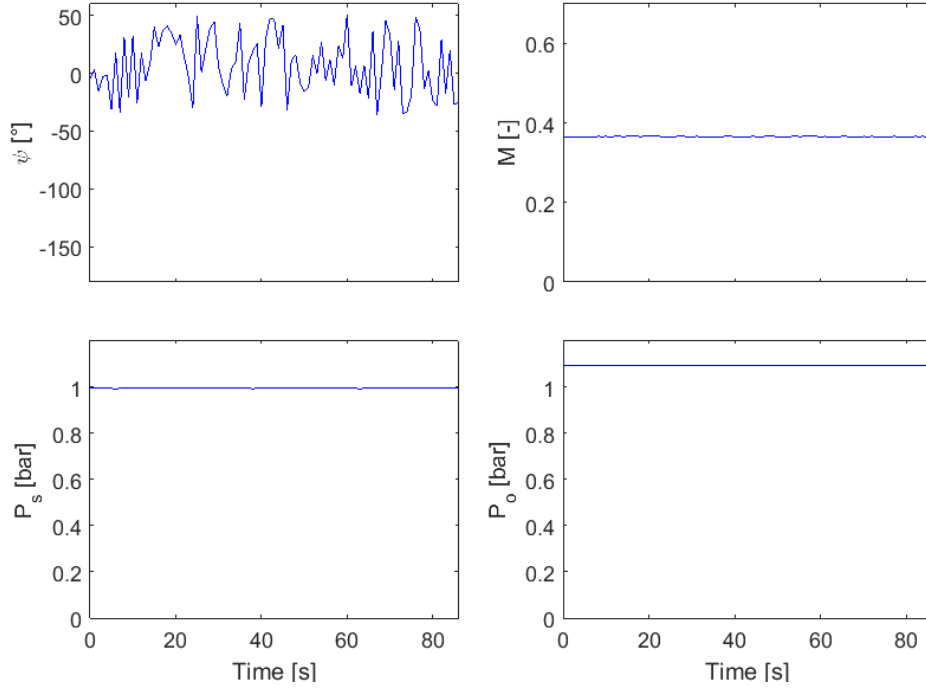


Figure 4.4: Flow quantities reconstruction with aerodynamic calibration script

In Figure 4.4, the result of flow quantities reconstruction from time-resolved pressure measurements can be perceived, however, it gives no idea of the method's quality. To solve this, a new feature is added to the script and it is described in the following section 4.1.1.

4.1.1. Modifications to Aerodynamic Calibration Script

The script was previously validated only for experimental data of a wedge probe with fixed angle between sensors (Delhayé, Paniagua, et al. 2010) and for this reason, alterations were required for compatibility purposes and additionally, some small features were included.

Namely, an overall update of the input system to match the new data and also to include the pitch angle was made. The latter will allow evaluation of pitch sequences angular data to further evaluate the effect of neglecting for the flow quantities retrieval.

A new option to create tests in resemblance to real conditions using calibration points is added. This allowed uncertainty analysis depicted in section 1.1.

Tests are generated the selection of angular calibration pressure values by a random order over the whole calibration range except on the extremities, in order to diminish the out of range number of points. Since this flow is known, a succeeding evaluation of flow quantities reconstruction error is possible.

To demonstrate the process, the same example is used. For it, data from calibrations at a pitch angle of $+5^\circ$ with added pressure error of $+5\text{mbar}$ and sensor position of $+1^\circ$ was used to generate the test on Figure 4.2.

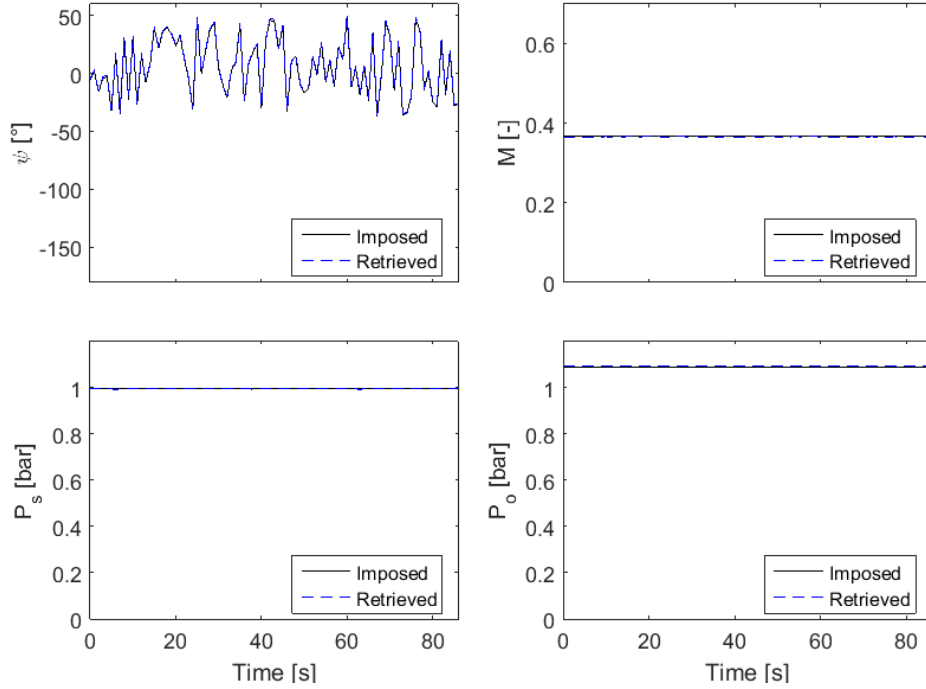


Figure 4.5: Three FRAP's imposed and retrieved flow quantities

For comparison, imposed test data and retrieved flow quantities are shown in Figure 4.5. A successful flow recovery is verified.

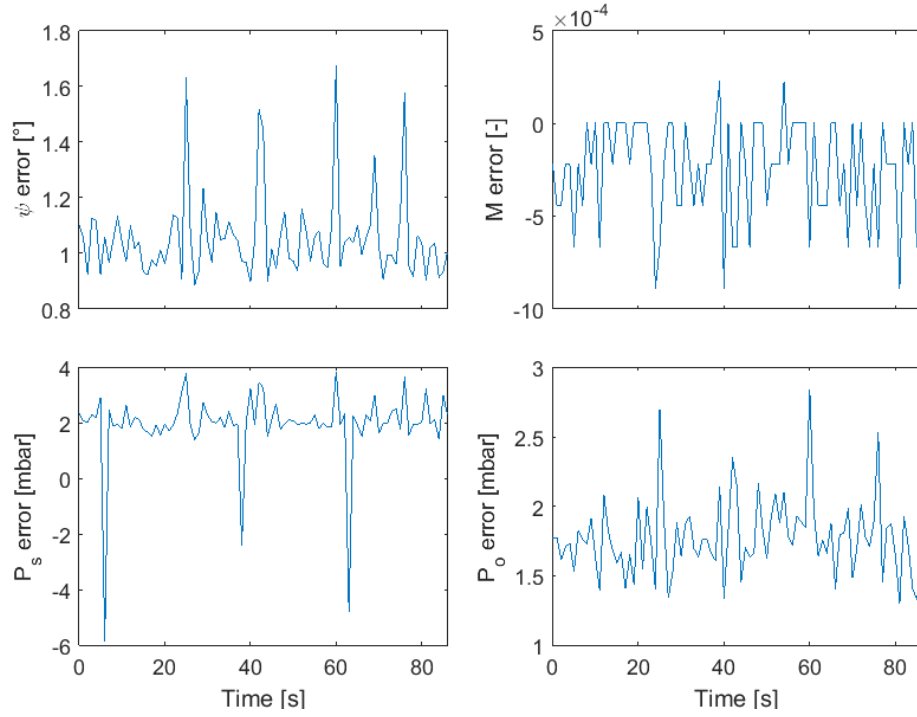


Figure 4.6: Three FRAP's error in flow quantities reconstruction

Finally, on Figure 4.6 error variation for the flow quantities is shown for the present example.

4.2. Configuration Evaluation

The present work requires a study of the best configuration with the available FRAP's inside a turbine's wind tunnel for 2D flow measurements.

Thusly, Table 4.1 presents a summary of angular calibrations performed to each probe.

<i>Probe</i>	<i>Yaw sequences</i>	<i>Mach number [-]</i>					<i>Pitch sequences</i>	<i>Mach Number [-]</i>		
DAO129A	5	0.000	0.199	0.342	0.452	0.565	1	-	0.332	-
DAO129B	5	0.021	0.201	0.340	0.458	0.560	-	-	-	-
DAO129C	5	0.133	0.238	0.358	0.457	0.568	-	-	-	-
DAO129D	5	0.136	0.237	0.368	0.474	0.554	3	0.143	0.366	0.540
DAO129E	5	0.144	0.245	0.366	0.469	0.578	-	-	-	-
DAO129F	5	0.139	0.248	0.367	0.472	0.595	-	-	-	-
DAO132A	5	0.138	0.252	0.374	0.478	0.595	-	-	-	-
DAO132B	4	0.137	0.239	0.357	0.467	-	1	-	0.356	-
DAO132D	5	0.134	0.249	0.371	0.48	0.601	-	-	-	-

Table 4.1: Angular calibration list by Mach number and measuring sequence

The first two probes have lower Mach number calibrations; therefore, in order to be assembled with one other probe for 2D flow measurements, they will require each at least two new calibrations.

As for the probes with Kulite® transducers, one is a Mach number calibration short for the upper range. Even though accordingly to CFD predictions, it is still within the calibration range, when considering possible measurements errors, a higher upper range calibration would be beneficial.

As far as Mach number calibrations proximity goes, the best combination is using probes DAO129F, DAO132A and DAO132D.

However, as mentioned in section 1.1, instead of using three probes in conjoint measurements, as an alternative, only one probe can perform three pressure measurements with a different angular position in each test. This method is also valid to use in the aerodynamic calibration script.

Advantages lie on a lower blockage effect and on a smaller number of devices to oversee during the experiments. An equally important point is the fact the each probe angular calibration was performed under a different static pressure hence; their combination induces errors because aerodynamic calibration equations only take into account one static pressure, in this case, the one of the central sensor.

4.2.1. Angle Between Sensors

According to (Morelli 2014) the most precise maps are obtained using an angle of 35° between sensors due to cells regular sizes but, depending on the selected sensors for the virtual three-hole probe and on the central amplification coefficient, these angles can be within 30° and 40° interval.

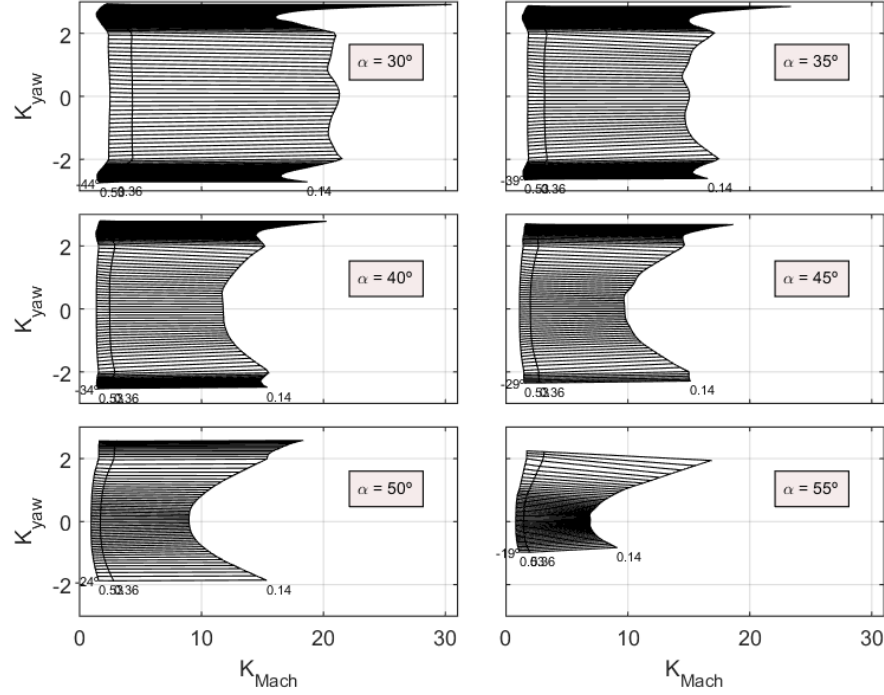


Figure 4.7: Zonal calibration map for different angles between sensors

Observing Figure 4.7, it is verified to be accurate that the ideal angle is around 30° and 40° , more specifically of 35° , for it keeps a wider range and every cell is distinguishable.

From an angle higher than 40° the zonal calibration maps cells are all also distinguishable but the range gets significantly shorter.

In conclusion, the best angular configuration appears to be around -35° , 0° and $+35^\circ$ for the left, central and right sensor respectively.

4.2.2. Central Amplification Coefficient K_z

As previously mentioned, this parameter is used to amplify pressure values measured solely by the central sensor and moreover, to obtain monotonous and quasi-linear calibration curves for K_{yaw} and K_{Mach} .

Optimization of amplification parameter k_z is consequently performed while studying monotony range and slopes of K_{yaw} and K_{Mach} . Monotony sets the uniqueness of the solution and slope improves precision, minimizing errors in the physical data evaluation.

The script builds dimensionless coefficients that describe how the monotony, accuracy and amplitude of the central range are affected by the variation of the k_z parameter. Their linear combination generates a function and its maximum corresponds to the optimum value of k_z , to be used to find the aerodynamic calibration coefficients:

$$Y = A_1 coeff_{K_{yaw}} + B_1 coeff_{K_{Mach}} + C_1 coeff_{K_{CentralAmplitude}} \quad (4.4)$$

Parameters A_1, B_1 and C_1 are set by the user accordingly to the weight to be given to each coefficient and their combination will determine the central amplification coefficient.

Central range amplitude is the amount of aerodynamic calibration coefficients calculated with the central sensor zone formula, thus its value is increased when the central amplification parameter k_z is higher. Achieving the right k_z will improve the calibration maps and provide distinguishable and well defined cells.

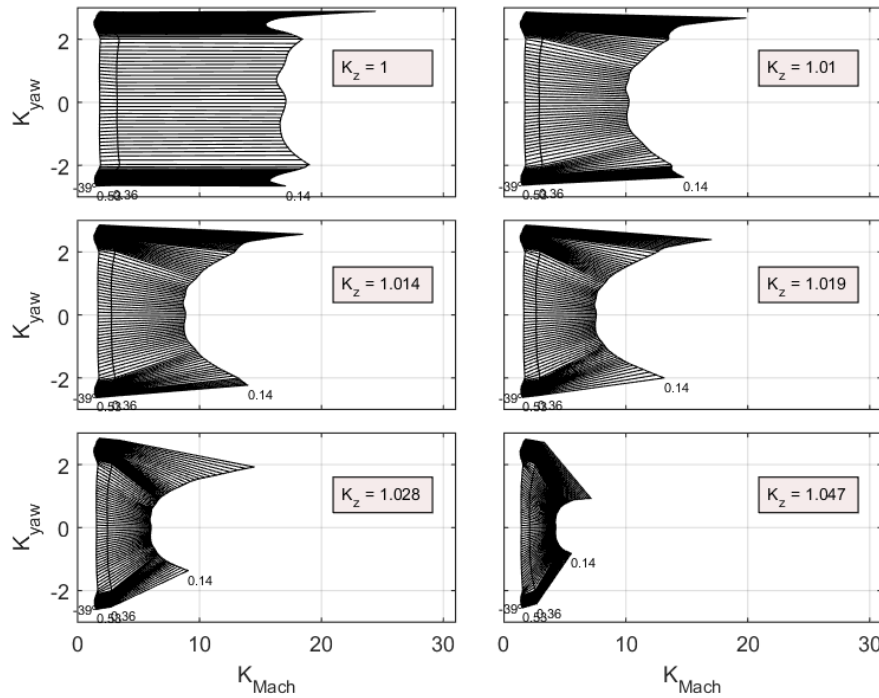


Figure 4.8: Zonal calibration map for different central amplification coefficients

On Figure 4.8, the best central amplification coefficient appears to be that of no amplification at all.

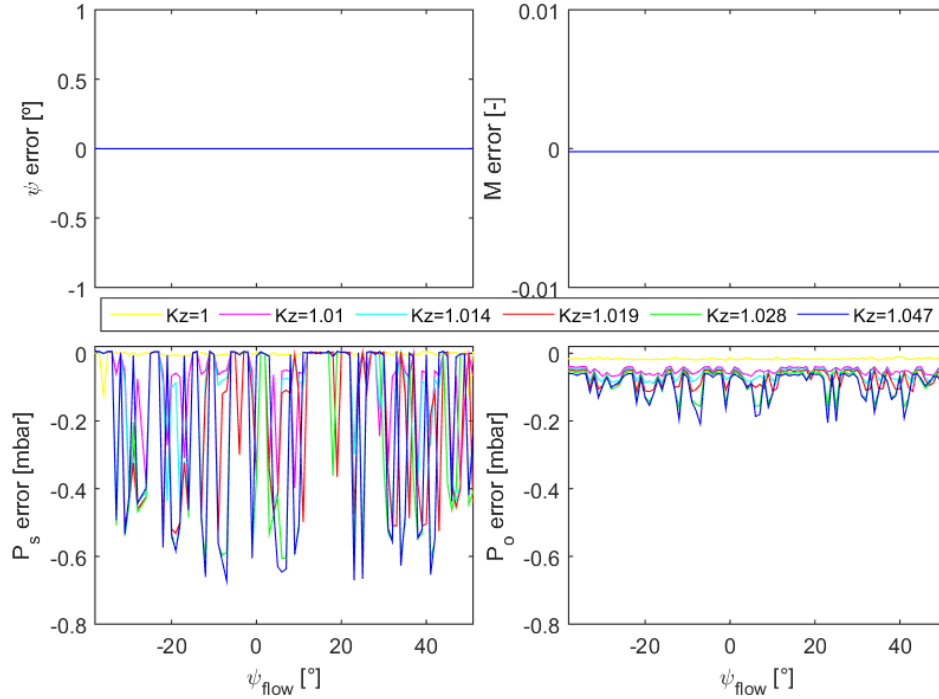


Figure 4.9: Flow quantities error for different central amplification coefficients

Such conclusion is supported by Figure 4.9, where despite no influence in retrieving yaw angle and Mach number, a higher the central amplification coefficient increases slightly the error peaks in retrieving static and total pressure.

4.3. Uncertainty Analysis

A new option added to the aerodynamic calibration script allows an uncertainty analysis through the comparison between error free and induced error flow recovery.

In continuity with the previous examples, FRAP DAO129D is again used, due to its pitch sequences calibration that will allow an uncertainty analysis of pitch angle effect, for a configuration with 35° angle between pressure sensors and a central amplification coefficient of 1.002.

It is important to mention that tests are generated only for the middle Mach number calibration to lower as much as possible the out of range points.

For this process, errors are added to the generated tests from angular calibration data, accordingly to the desired analysis. Then, these tests are used for the reconstruction the flow quantities with a probe configuration unaware of this errors, as it happens in a real test, i.e. no pressure errors, sensors' angles are equal to the intended positions and the pitch angle variations are neglected, thusly considering a constant null pitch angle for flow recovery.

4.3.1. Pressure Readings Error

An error of $\pm 5\text{mbar}$ is added alternatively to each sensor calibration data used to generate tests, Figure 4.10.

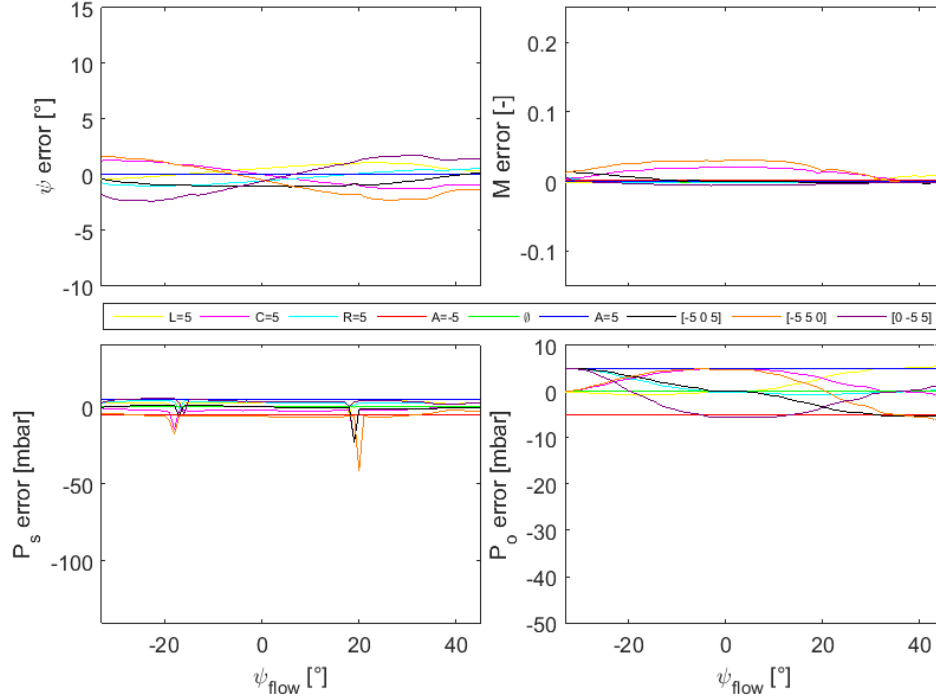


Figure 4.10: Flow quantities error for pressure readings error of ± 5 mbar

Pressure errors have an influence of $\pm 3^\circ$ in yaw angle and less than 0.05 in Mach number retrieval.

In total and static pressure, the error maximum amplitude is equal to its value, and it is more or less constant if the induced error is equal in all sensors during the measurements.

4.3.2. Sensor Angle Position Error

Contrarily to fixed sensors probes, this method, whether using three probes at the same time or one probe with different angular positions in three tests, requires for every test an angular movement prone to positioning errors. In order to evaluate this effect, errors of 5° in the sensor position during angular calibration are inserted for the selection of points for the tests generation, Figure 4.11.

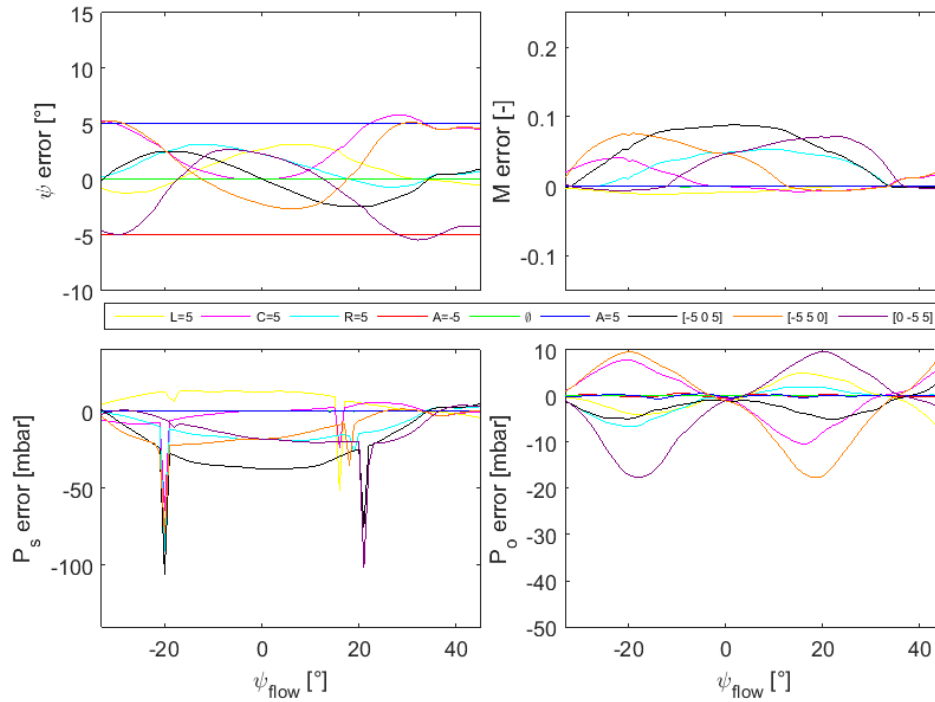


Figure 4.11: Flow quantities error for sensor position error of $\pm 5^\circ$

Sensor angular positioning error shall have an expected higher effect on the retrieval of yaw angle, which can be slightly higher than the induced error itself.

Mach number error is also rather high, it can reach 0.1. However, the applied error magnitude is to some extent inflated.

In general, higher errors appear for different errors between angles.

4.3.3. Pitch Angle Error

The flow in turbomachines is fully three-dimensional; however, pressure measurements with three sensors are currently only able to characterize flow variations in one direction, yaw-wise, leaving the pitch angle variation unknown. With regard to this, the influence on the reconstruction of the other flow quantities is analysed for pitch angle variations between $\pm 30^\circ$, Figure 4.12.

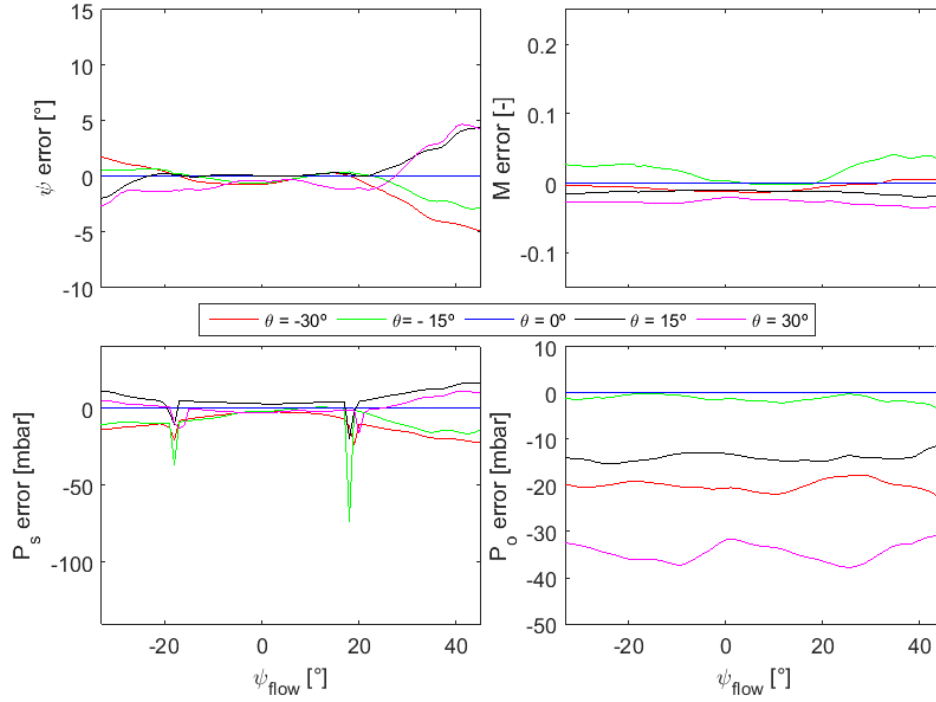


Figure 4.12: Flow quantities error for pitch angle variation of $\pm 30^\circ$

In comparison to the others errors, this one has the lowest impact in yaw angle retrieval, which is smaller than 1° for flow yaw angle variations between $\pm 20^\circ$. Nevertheless, the error can reach $\pm 5^\circ$ for a flow yaw angle higher than 45° .

Static pressure error is more or less symmetric and it increases for increasing pitch and yaw angle.

Pitch angle effect decreases greatly the acquired pressure due to incidence variation and this effect is heavier on positive rather than on the negative pitch angles.

A method to correct this effect is described in (Schlienger, et al. 2002) in which it is claimed three-dimensional flow can be characterized upon using five pressure measurements at different angular positions. However, since it does not take into account the Mach number variation, a flow quantity would still be uncharacterized.

4.3.4. Combination of Possible Errors

In a test campaign, several errors will take place at the same time and there is no clear way of linking them to their source and isolate them. For this reason, known possible errors to occur are considered and their conjoint effect is analysed in order to give an idea of expectations for flow reconstruction in real test conditions, Figure 4.13.

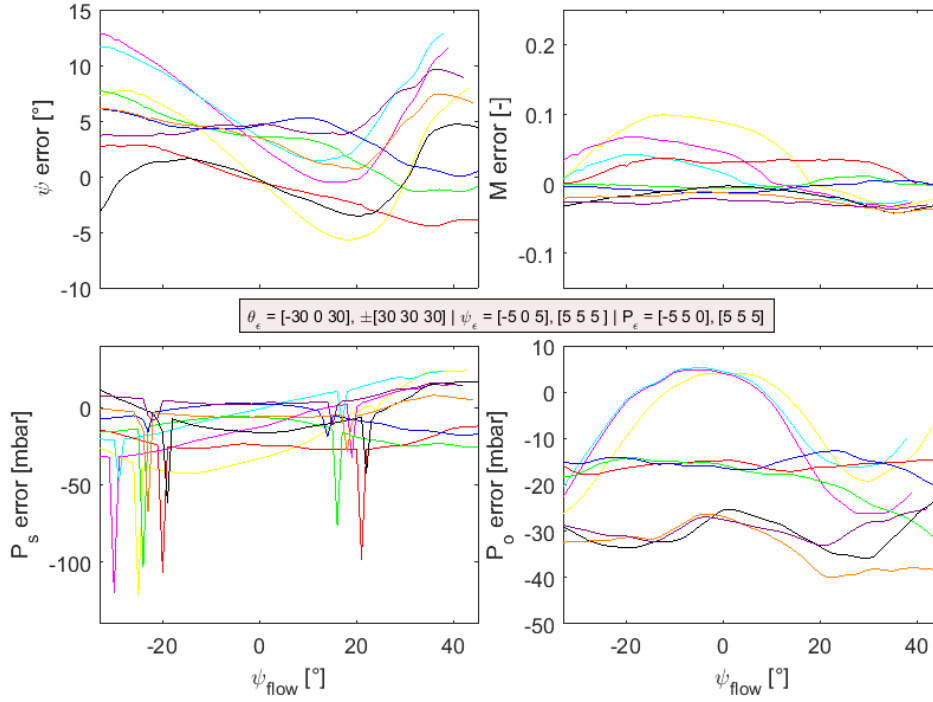


Figure 4.13: Flow quantities error for combined known sources of errors

Average yaw angle error is smaller than 5° , nevertheless it can reach 13° for extreme yaw and pitch angles in case a difference pitch angle is being measured in each sensor for the same time domain.

For the current example, sensors pitch angles were of -30° , 0° and $+30^\circ$ and as results, the highest errors were obtained for this configuration as well as a flow recovery higher than one.

Average and maximum error values in terms of studied flow quantities can be seen in Table 4.2.

Error	φ [°]	M [-]	P_o [mbar]	P_s [mbar]
Mean	4.013	0.0447	20.61	17.87
Max	13.01	0.2072	48.71	137.2

Table 4.2: Average and maximum flow quantities error for inserted pressure, sensor and pitch angle variation

5 Conclusions

Data processing of static and angular calibration of fast-response pressure probes is concluded. In it, an angular deviation was detected and corrected and static calibration coefficients were recomputed for a total pressure acquisition at null yaw and pitch angle. A higher than one recovery factor was observed in Measurement Specialties™ transducers probes for low Mach numbers where drift is present. Probes with Kulites® transducers show a more reliable calibration and response to pressure fluctuations.

As for the aerodynamic calibration, a configuration evaluation for placement of a 2D flow measuring probe arrangement in the turbine test rig demonstrated that angles between sensors around 30° and 40° provide the most advantageous calibration maps, in terms of distinguishable cells for flow quantities reconstruction and maintaining an adequate yaw angle calibration range. However, for the majority of tested probe combinations, the best calibration maps were obtained with 35° between sensors. Moreover, this was the configuration used in uncertainty analysis for induced errors where they were kept to a minimum within a yaw angle range of $\pm 20^\circ$ for sensors arranged at -35°, 0° and +35°.

Pitch angle variations have a large effect on the reconstruction of flow direction by yaw angle and it is especially severe if a different angle is being measured at each sensor.

The choice of using simultaneously three probes in close proximity in the test rig will provide pressure measurements with a minor pitch influence. However, blockage effect shall be reduced if probes are displaced at different circumferential positions instead. This distribution is also an advantage when measuring flows with large radial components.

Lastly, the use of a single probe at different angular positions for each measurement appears to raise the biggest chain of errors due to variations between measurements, as probe angular mispositioning, differences in pressure and temperature inside the test rig, pitch angle variation, amongst others, will highly condition the overall accuracy of this method. Notwithstanding, this configuration provides the smallest blockage effects due to probe's small size and reduces the small errors of combining different probes calibrated under slightly different flow conditions.

6 Recommendations for Future Work

An in-situ calibration, described in section 3.1.2, is necessary for accurate testing in the turbine test rig, with regard to its high temperature and pressure transients.

Furthermore, the high influence of pitch angle variations above $\pm 15^\circ$ on 2D flow characterization demand a correction of this angular sensitivity.

Moreover, even if no correct is applied, in case of a combination of a single probe at different angular positions is chosen, a perfect synchronization of measurements is advised in order to minimize the pitch angle effects, considerably higher when different in each sensor.

7 List of References

Anderson Jr., J. D. *A History of Aerodynamics and Its Impact on Flying Machines*. UK: Cambridge University Press, 1997.

Anthoine, J., et al. *Measurement Techniques in Fluid Dynamics: An Introduction*. 3rd edition. Rhode-Saint-Genèse: the von Kármán Institute for Fluid Dynamics, 2009.

Bonetti, G. *Evaluation of miniaturized fast response probes*. Rhode-Saint-Genèse: the von Kármán Institute for Fluid Dynamics, 2013.

Brouckaert, J. -F. *Development of Fast Response Aerodynamic Pressure Probes for Time-Rosolved Measurements in Turbomachines*. Rhode-Saint-Genèse: the von Kármán Institute for Fluid Dynamics, 2014.

Bryer, D. W., and R. C. Pankhurst. *Pressure-probe methods for determining wind speed and flow direction*. London: Her Majesty's Stationary Office, 1971.

Delhaye, D. *Steady and unsteady flow measurements downstream of a transonic HP turbine stage*. Louvain: Université Catholique de Louvain, 2006.

Delhaye, D., G. Paniagua, J. M. Fernández Oro, and R. Dénos. "Enhanced performance of fast-response 3-hole wedge probes for transonic flows in axial turbomachinery." *Experiments in Fluids*, 15 June 2010: 163-177.

Dénos, R. "Influence of temperature transients and centrifugal force on fast-response pressure transducers." *Experiments in Fluids*, 9 April 2002: 256-264.

Denton, J. D. "Loss Mechanisms in Turbomachines." *ASME Journal of Turbomachinery*, 1 October 1993: 521-652.

García, D. *Calibration of temperature and pressure probes for turbine testing*. Rhode-Saint-Genèse: the von Kármán Institute for Fluid Dynamics, 2014.

Gossweiler, C. "Unsteady Measurements with Fast Response Probes." *The von Kármán Lecture Series 1996-01*. Rhode-Saint-genèse: the von Kármán Institute for Fluid Dynamics, 1996.

Kupferschmied, P., C. Gossweiler, and G. Gyarmathy. "Aerodynamic Fast Response Probe Measurement Systems: State of Development, Limitations and Future Trends." *Proceedings of the 12th Symposium on Measuring Techniwues for Transonic and Supersonic Flows in Cascades and Turbomachines*. Prague, Czech Republic, 1994.

Kupferschmied, P., P. Koppel, W. Gizzi, C. Roduner, and G. Gyarmathy. "Time-resolved flow measurements with fast-response aerodynamic probes in turbomachines." *Measurement Science and Technology*, November 2000: 1036-1054.

Lavagnoli, S. On the Aerothermal Flow Field in a Transonic HP Turbine Stage with a Multi-Profile LP Stator Vane. Rhode-Saint-Gen  se: the von K  rm  n Institute for Fluid Dynamics, 2012.

Lenherr, C. *High Temperature Fast Response Aerodynamic Probe*. Zurich: Swiss Federal Institute of Technology, 2010.

Lienhard, J. H. Synopsis of Lift, Drag, and Vortex Frequency Data for Rigid Circular Cylinders. Washington State University, 1966.

Mansour, M. A 48kHz Bandwidth, 1.8mm Diameter Entropy Probe for Aerothermal Loss Measurements in Turbomachinery Flows. Zurich: Swiss Federal Institute of Technology, 2009.

Morelli, A. *Advanced data processing of multi-hole directional probes*. Rhode-Saint-Gen  se: the von K  rm  n Institute for Fluid Dynamics, 2014.

Paniagua, G. *Investigation of the Steady and Unsteady Performance of a Transonic HP Turbine*. Rhode-Saint-Gen  se: the von K  rm  n Institute for Fluid Dynamics, 2002.

Pfau, A. *Loss Mechanisms in Labyrinth Seals of Shrouded Axial Turbines*. Zurich: Swiss Federal Institute of Technology, 2003.

Pfau, A., J. Schlienger, A. I. Kalfas, and R. S. Abhari. "Virtual Four Sensor Fast Response Aerodynamic Probe(FRAP)." *The 16th Symposium on Measuring Techniques in Transonic and Supersonic Flow in Cascades and Turbomachines*. Cambridge, United Kingdom, 2002.

Schlienger, J., A. Pfau, A. I. Kalfas, and R. S. Abhari. "Single Pressure Transducer Probe for 3D Flow Measurements." *The 16th Symposium on Measuring Techniques in Transonic and Supersonic Flow in Cascades and Turbomachines*. Cambridge, United Kingdom, 2002.